Biochemical Journal (2020) **477** 4527–4541
https://doi.org/10.1042/BCJ20200776

PORTLAND PRESS

Research Article

Crystal structures of ORFV125 provide insight into orf virus-mediated inhibition of apoptosis

Chathura D. Suraweera[1], Mark G. Hinds[2,*] and Marc Kvansakul[1]

[1]Department of Biochemistry and Genetics, La Trobe Institute for Molecular Science, La Trobe University, Melbourne, Victoria 3086, Australia; [2]Bio21 Molecular Science and Biotechnology Institute, The University of Melbourne, Parkville, Australia

Correspondence: Marc Kvansakul (m.kvansakul@latrobe.edu.au)

OPEN ACCESS

Premature apoptosis of cells is a strategy utilized by multicellular organisms to counter microbial threats. Orf virus (ORFV) is a large double-stranded DNA virus belonging to the *poxviridae*. ORFV encodes for an apoptosis inhibitory protein ORFV125 homologous to B-cell lymphoma 2 or Bcl-2 family proteins, which has been shown to inhibit host cell encoded pro-apoptotic Bcl-2 proteins. However, the structural basis of apoptosis inhibition by ORFV125 remains to be clarified. We show that ORFV125 is able to bind to a range of peptides spanning the BH3 motif of human pro-apoptotic Bcl-2 proteins including Bax, Bak, Puma and Hrk with modest to weak affinity. We then determined the crystal structures of ORFV125 alone as well as bound to the highest affinity ligand Bax BH3 motif. ORFV125 adopts a globular Bcl-2 fold comprising 7 α-helices, and utilizes the canonical Bcl-2 binding groove to engage pro-apoptotic host cell Bcl-2 proteins. In contrast with a previously predicted structure, ORFV125 adopts a domain-swapped dimeric topology, where the α1 helix from one protomer is swapped into a neighbouring unit. Furthermore, ORFV125 differs from the conserved architecture of the Bcl-2 binding groove and instead of α3 helix forming one of the binding groove walls, ORFV125 utilizes an extended α2 helix that comprises the equivalent region of helix α3. This results in a subtle variation of previously observed dimeric Bcl-2 architectures in other poxvirus and human encoded Bcl-2 proteins. Overall, our results provide a structural and mechanistic basis for orf virus-mediated inhibition of host cell apoptosis.

Introduction

Apoptosis is a form of programmed cell death utilized by multicellular organisms as a defence mechanism against invading pathogens [1] and viruses have evolved multiple strategies to antagonize this process [2]. One such strategy utilized to subvert host cell apoptosis is the application of molecular mimicry to produce structural, functional and sequence homologues of cellular pro-survival proteins including B-cell lymphoma 2 (Bcl-2) family proteins [3]. Viral Bcl-2 proteins obstruct premature host cell death and are critical for successful infection and proliferation [4]. Bcl-2 family proteins are key regulators of intrinsic or mitochondria-mediated apoptosis [5] and typically contain one or more conserved sequence motifs referred to as Bcl-2 homology (BH) motifs [6], though these are frequently absent from virus-encoded homologues [3].

Bcl-2 family proteins comprise both pro-survival and pro-apoptotic Bcl-2 proteins [4] and the interplay between the two groups governs cellular fate [5]. The cellular pro-survival Bcl-2 proteins include Bcl-2, Bcl-x_L, Bcl-w, Bcl-B, Mcl-1 and A1 [7], which bear multiple BH motifs in addition to a C-terminal hydrophobic transmembrane region that targets proteins to the mitochondrial outer membrane [8]. Pro-apoptotic Bcl-2 proteins can be sub-divided into two phylogenetically distinct groups, the multi motif pro-apoptotic proteins such as Bak, Bax and Bok or the BH3-only proteins which only have a conserved BH3 motif [9]. The BH3-only proteins include Bad, Bid, Bik, Bim, Bmf, Hrk, Noxa and Puma. Bax, Bak (or Bok) are critical for intrinsic apoptosis and many hypotheses for the

*Co-senior author.

Received: 2 October 2020
Revised: 6 November 2020
Accepted: 11 November 2020

Accepted Manuscript online: 11 November 2020
Version of Record published: 3 December 2020

Biochemical Journal (2020) 477 4527–4541
https://doi.org/10.1042/BCJ20200776

mechanism of Bax–Bak induced apoptosis have been put forth. Two main mechanisms have been proposed: BH3-only protein neutralization of pro-survival Bcl-2 proteins and direct BH3-only activation of Bak and Bax [10,11]. Pro-survival Bcl-2 proteins interact with the BH3 motif of pro-apoptotic Bcl-2 proteins via their conserved hydrophobic ligand-binding groove to prevent cell death [12]. Bax and Bak activation is crucial for the progression of mitochondrially mediated apoptosis and upon their activation oligomerize [13] at the mitochondrial outer membrane to form pore-like structures [14]. Pore formation at the mitochondrial surface enables the release of cytochrome *c* to bind the adaptor protein APAF-1 to form the apoptosome [15] that activates the caspase cascade leading to cellular destruction. Key to the neutralization of pro-survival Bcl-2 proteins is the interactions between the BH3 motif of pro-apoptotic proteins and pro-survival Bcl-2 proteins and these have been extensively characterized [9]. The presence of viral Bcl-2 (vBcl-2) homologues prevents Bak and Bax activation and subsequent induction of apoptosis to keep cells alive for viral replication [16].

ORF virus (ORFV) is an epitheliotropic virus belonging to the family of *poxviridae*, and is considered the prototypical member of the genus *parapoxviridae*. Other members of the *parapoxviridae* genus include Bovine papular stomatitis virus (BPSV) and Pseudocowpox virus (PCPV) [17]. ORFV primarily infects sheep and goats causing highly contagious skin lesions localized on lips, toes, nostrils and udders [18]. This disease is self-limiting, infected animals clear the infection within 3–4 weeks and develop lifelong immunity against this virus. ORFV also infects humans via handling of infected animals or contaminated equipment and causes skin lesions that last 3–4 weeks [18]. As a large double-stranded DNA virus the ORFV genome is ∼140 kbp in size and encodes numerous immunomodulatory genes including the anti-apoptotic protein ORFV125 [19]. ORFV125 is a 173 residue putative Bcl-2 like protein known to inhibit mitochondrially mediated host cell apoptosis during infection [19]. Sharing relatively little sequence identity with mammalian Bcl-2 proteins ORFV125 lacks obvious BH motifs [20] and immunoprecipitates with the BH3-only proteins Bik, Bim, Puma, Noxa and Hrk as well as with pro-apoptotic Bax [20]. Homology modelling suggested that ORFV125 adopts a monomeric globular helical bundle fold comprising 8 α-helices similar to murine Bcl-x_L, human Bcl-w and Mcl-1 [19]. We now report the structural and biochemical characterization of ORFV125. Our data show that ORFV125 adopts a domain-swapped dimeric structure similar to other poxvirus encoded Bcl-2 homologues and is able to bind BH3 motif peptides from Hrk, Puma, Bak and Bax using the canonical Bcl-2 ligand-binding groove. Our findings establish a structural and mechanistic basis for ORFV125 mediated inhibitor of apoptosis.

Experimental (materials and methods)

Protein expression and purification

Synthetic cDNA encoding for codon-optimized ORFV125 (Uniprot Accession number W6EVU4) lacking the 30 C-terminal residues was cloned into the bacterial expression vector pGex-6p-1 (GenScript) and is subsequently referred to as ORFV125. Recombinant ORFV125 was expressed in C41(DE3) cells in 2YT medium supplemented with 1 mg/ml ampicillin at 37°C in a shaking incubator until an OD_{600} of 0.6 was reached. The protein expression was induced by adding isopropyl β-D-1-thiogalactopyranoside (IPTG) to a final concentration of 0.75 mM for 18 h at 20°C. Bacterial cells were harvested by centrifugation at 5000 rpm (JLA 9.1000 rotor, Beckman Coulter Avanti J-E) for 20 min and re-suspended in 100 ml lysis buffer A (50 mM Tris pH 8.0, 300 mM NaCl, 5 mM DTT (dithiothreitol) and 1% Tergitol. The cells were homogenized using an Avestin EmulsiFlex homogenizer and lysed using sonication (programme 7, Fisher Scientific™ Model 705 Sonic Dismembrator) and the resultant lysate was transferred into SS34 tubes for further centrifugation at 18 000 rpm (JA-25.50 rotor, Beckman Coulter Avanti J-E) for 30 min. The supernatant was loaded onto a 5 ml glutathione sepharose 4B column (GE Healthcare) equilibrated with buffer A. After sample application, the column was washed with 150 ml of buffer A and removal of the GST tag was performed on-column by adding HRV 3C protease overnight at 4°C. The cleaved protein was eluted using buffer A and concentrated using a centrifugal concentrator with 3 kDa molecular mass cut-off (Amicon® Ultra 15) to a final volume of 3 ml. Concentrated ORFV125 was subjected to size-exclusion chromatography using a Superdex S200 increase 10/300 column mounted on an ÄKTA Pure system (GE Healthcare) equilibrated in 25 mM HEPES pH 7.5, 150 mM NaCl and 5 mM TCEP (Tris(2-carboxyethyl)phosphine hydrochloride). The final sample purity was estimated to be higher than 95% based on SDS–PAGE analysis. Appropriate fractions were pooled and concentrated using a centrifugal concentrator with 3 kDa molecular mass cut-off (Amicon ® Ultra 15) to a final concentration of 6.4 mg/ml.

Selenomethionine labelled protein was expressed in minimal media supplemented with 60 mg/l of Selenomethionine as previously described [21] and purified as above.

Measurement of dissociation constants

Binding affinities were measured using a MicroCal iTC200 system (GE Healthcare) at 25°C using wild type ORFV125 in 25 mM HEPES pH 7.5, 150 mM NaCl, 10 mM TCEP at a final concentration of 60 μM. BH3 motif peptide ligands were used at a concentration of 600 μM except Bak (800 μM) and Puma (700 μM) and titrated using 19 injections of 2.0 μl of ligand. All affinity measurements were performed in triplicate. Protein concentrations were measured using a Nanodrop UV spectrophotometer (Thermo Scientific) at a wavelength of 280 nm. Peptide concentrations were calculated based on the dry peptide weight after synthesis. The BH3 motif peptides used were commercially synthesized and were purified to a final purity of 95% (GenScript) and based on the human sequences shown in Table 1 and described previously [22].

Crystallization and structure determination

Crystals of *apo*-ORFV125 were obtained at a protein concentration of 6.0 mg/ml. Crystals for ORFV125: Bax BH3 complex were obtained by mixing ORFV125 with human Bax 28-mer peptide at a 1 : 1.25 molar ratio as described [23] and concentrated using a centrifugal concentrator with 3 kDa molecular mass cut-off (Amicon ® Ultra 0.5) to 6.4 mg/ml. The concentrated protein was immediately used for crystallization trials using commercial sparse matrix screens in 96 well-sitting drop trays (Swissic, Neuheim, Switzerland).

ORFV125: Bax BH3 crystals were grown by the sitting drop vapour diffusion method at 20°C in 0.2 M Magnesium chloride hexahydrate, 0.1 M Bis-Tris pH 5.5, 25% PEG 3350. The crystals were flash cooled at −173°C in the mother liquor. The ORFV125: Bax BH3 complex formed single rod-shaped crystals belong to space group I2 with $a = 69.51$ Å, $b = 45.56$ Å, $c = 105.96$ Å, $\alpha = 90.00$ Å, $\beta = 106.05$ Å, $\gamma = 90.00$ Å in orthorombic crystal system. All diffraction data were collected at the Australian Synchrotron MX2 beamline [24] using an Eiger detector with an oscillation range 0.1° per frame with a wavelength of 0.9537 Å. The diffraction data were integrated using XDS [25] and scaled using AIMLESS [26]. Selenomethionine labelled ORFV125: Bax BH3 crystals were obtained in the same crystallization condition as described above for the unlabelled complex. Anomalous diffraction data were collected at the MX1 beamline [27] at the Australian Synchrotron using an Eiger detector with an oscillation range 0.1° per frame with a wavelength of 0.97710 Å, integrated using XDS [25], and scaled using Aimless [26]. The structure was phased by single-wavelength anomalous diffraction (SAD) using Selenium atoms. Five sites were located using Shelx [28] and phased using AutoSol in Phenix [29,30] with a figure of Merit of 0.30. The initial map was built using Phenix autobuild, and the resultant structure was used for molecular replacement of native ORFV125: Bax using PHASER [31]. ORFV125: Bax BH3 crystals contain two molecules of ORFV125 and two Bax BH3 peptide, with 41.05% solvent content and

Table 1. Isothermal titration colorimetry binding affinities of ORFV virus Bcl-2 homologue ORFV125 with pro-apoptotic BH3 motif peptides from human.

Peptide	WT K_D (nM)	Sequence
Bak	5802 ± 737	67-PSSTMGQVGRQLAIIGDDINRRYDSE-92
Bax	682 ± 38	50-VPQDASTKKLSECLKRIGDELDSNMELQ-77
Bok	NB	59-VPGRLAEVCAVLLRLGDELEMIRPSV-84
Bad	NB	103-NLWAAQRYGRELRRMSDEFVDSFKKG-128
Bid	NB	79-SESQEDIIRNIARHLAQVGDSMDRSIPPGLVNGL-104
Bik	NB	51-MEGSDALALRLACIGDEMDVSLRAP-75
Bim	NB	51-DMRPEIWIAQELRRIGDEFNAYYARR-76
Bmf	NB	125-QHQAEVQIARKLQCIADQFHRLHVQQ-151
Hrk	1912 ± 66	26-RSSAAQLTAARLKAIGDELHQRTMWR-51
Noxa	NB	18-PAELEVECATQLRRFGDKLNFRQKLL-43
Puma	1753 ± 388	130-EEQWAREIGAQLRRMADDLNAQYERR-155
Beclin-1	NB	105-DGGTMENLSRRLKVTGDLFDIMSGQT-130

All K_D values (in nM) are the means of three replicates with standard error and 'NB' denotes No binding. Start and end residue as well as complete sequence for each BH3 motif peptide used is shown.

Biochemical Journal (2020) 477 4527–4541
https://doi.org/10.1042/BCJ20200776

final TFZ and LLG values of 22.3 and 1276.07, respectively. The final model of ORFV125: Bax BH3 was built manually over several cycles using Coot [32] and refined using PHENIX with final R_{work}/R_{free} of 23.3/25.9, with 99% of residues in the favoured region of the Ramachandran plot and no outliers.

apo-ORFV125 crystals were obtained in 0.2 M Sodium potassium tartrate, 0.1 M Bis-Tris propane pH 6.5, 20% PEG 3350. The crystals were flash cooled at −173°C in mother liquor supplemented with 20% ethylene glycol. The *apo*-ORFV125 crystals formed single trigonal bipyramidal crystals belong to space group $P6_222$ with $a = 106.25$ Å, $b = 106.25$ Å, $c = 60.72$ Å, $\alpha = 90.00$ Å, $\beta = 90.00$ Å, $\gamma = 120.00$ Å in the hexagonal crystal system. Diffraction data collection, integration and scaling were performed as described above. Molecular replacement was performed using the Phenix PhaserMR [29–31] pipeline with the previously solved ORFV125: Bax BH3 structure as a search model. *apo*-ORFV125 crystals contained one molecule of ORFV125 in the asymmetric unit, with 43% solvent content and final TFZ and LLG values of 11.4 and 93.60, respectively. The final model of *apo*-ORFV125 was built manually over several cycles using Coot [32] and refined using PHENIX [29,30] with final R_{work}/R_{free} of 24.4/26.0, with 99% of residues in the favoured region of the Ramachandran plot and no outliers. All images for *apo*-ORFV125 and ORFV125: Bax BH3 complexes were generated using PyMOL molecular graphic system version 1.8.6.0 (Schrödinger, LLC, New York, U.S.A.). All software were accessed through the SBGrid suite [33]. Co-ordinate files have been deposited in the Protein Data Bank under the accession code 7ADS and 7ADT. All raw diffraction images were deposited on the SBGrid Data Bank using their PDB accession numbers [34].

Analytical size-exclusion chromatography

Analytical size-exclusion chromatography was performed using a Superdex S75 3.2/300 column equilibrated in 25 mM HEPES pH 7.5, 150 mM NaCl and 5 mM TCEP as described above. The column was calibrated using three protein molecular mass markers (1 mg ml^{-1} Albumin (66 kDa), 2 mg ml^{-1} carbonic anhydrase (29 kDa) and 2 mg ml^{-1} cytochrome c (12 kDa)) (Sigma–Aldrich) dissolved in the same buffer as ORFV125. ORFV125 at a concentration of 3.0 mg ml^{-1} was then injected, and all elution profiles of the chromatograms were recorded.

Sequence alignment

Sequence alignments were performed using MUSCLE [35] (https://www.ebi.ac.uk/Tools/msa/muscle/) with the default settings.

Results

ORFV125 was identified as a putative Bcl-2 homologue via database searches by its sequence similarity to other poxvirus encoded Bcl-2 proteins such as VACV F1L (9.7% identity), MYXV M11L (11.2% identity) as well as cellular Bcl-x_L (15.7% identity) (Figure 1) [19]. It was previously reported that ORFV125 localized to the mitochondrial outer membrane using its C-terminal hydrophobic transmembrane region and was able to inhibit mitochondrially mediated apoptosis at multiple points in the signalling pathway [19,20]. However, the interactions of ORFV125 with host pro-apoptotic Bcl-2 proteins and the structural basis of apoptosis inhibition remained to be clarified. To understand the molecular and structural basis of apoptosis inhibition by ORFV125, we systematically investigated the structure and ability of recombinantly expressed and purified ORFV125 to bind to peptides spanning the BH3 motif region of human pro-apoptotic Bcl-2 proteins using isothermal titration colorimetry (ITC) (Figure 2, Table 1). ORFV125 displayed a highly selective repertoire of interactions with pro-apoptotic BH3 motif peptides, bound Bax BH3 (682 nM) with modest affinity and had weak affinity to Bak BH3 (5802 nM), Puma BH3 (1753 nM) and Hrk BH3 (1912 nM). No significant affinities were detected for all other tested BH3 motif peptides including the previously reported interactors Bim and Bik [20], or for the autophagy regulator Beclin-1.

To understand the structural basis of ORFV125 modulated inhibition of apoptosis we determined the crystal structures of *apo*-ORFV125 and its complex bound to its highest affinity ligand, Bax BH3 motif peptide (Figure 3a,b, Table 2). Despite sharing only modest sequence identity with its cellular counterparts, ORFV125 adopts the conserved Bcl-2 fold comprising seven α-helices (Figure 3a), with helices α2–α5 forming the canonical hydrophobic ligand-binding groove for BH3 motif peptides (Figure 3a,b) [8]. The crystal structure of *apo*-ORFV125 revealed a domain-swapped dimeric configuration that has been observed in several other poxviral Bcl-2 homologues including VACV F1L (Figure 3c) [36], VARV F1L [37], TANV16L (Figure 3d) [38] and DPV022 (Figure 3e) [39]. In the domain-swapped dimer, the α1 helix of one protomer is swapped with the α1

Biochemical Journal (2020) **477** 4527–4541
https://doi.org/10.1042/BCJ20200776

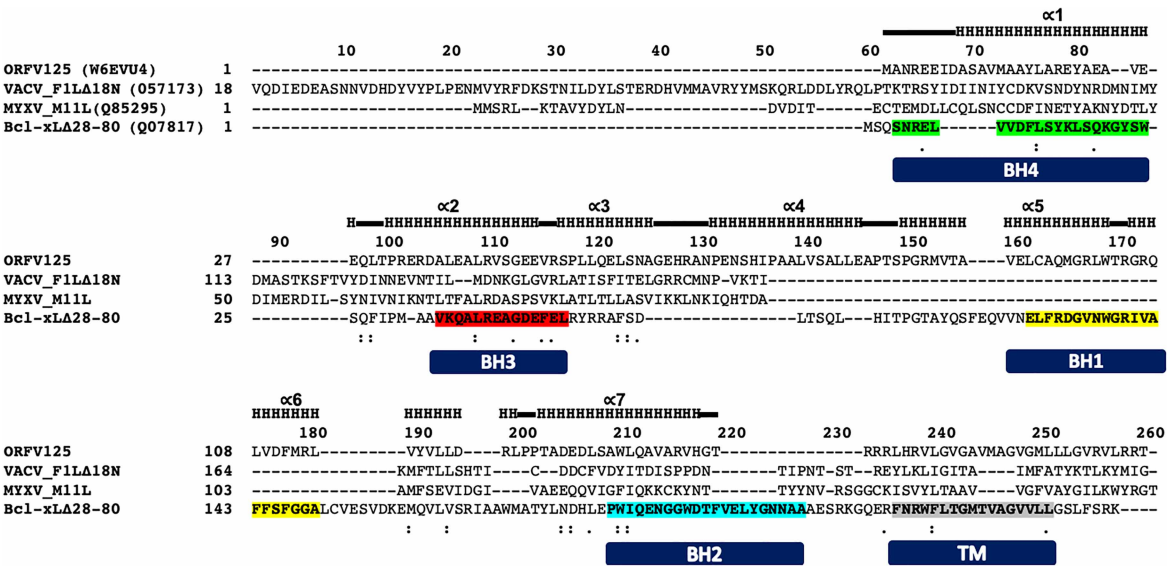

Figure 1. Sequence alignment of ORFV125 with pro-survival Bcl-2 family members.

The sequences of orf virus apoptosis regulator ORFV125 (uniprot accession number: W6EVU4), vaccinia virus F1L (uniprot: O57173), myxomavirus M11L (uniprot: Q85295) and human Bcl-x_L (uniprot: Q07817) were aligned using MUSCLE [35]. Secondary structure elements are marked based on the crystal structure of ORFV125, and BH motifs of Bcl-x_L highlighted (BH4 (bright green), BH3 (red), BH1 (yellow), BH2 (turquoise), transmembrane region (TM)(grey)) and shown in bold [7]. The helical regions are marked 'H' and unstructured loops by a bar above the sequence, with highly conservative substitutions indicated by ':' and conserved substitutions indicated by '.'.

helix of the neighbouring protomer (Figure 3a). To compare the differences between a single chain of ORFV125 and dimeric ORFV125 with previously reported domain-swapped dimeric Bcl-2 homologues in poxviruses including VACV F1L, VARV F1L, TANV16L and DPV022 (Figure 3c–e), we superimposed their Cα backbone with that of ORFV125. This yielded rmsd values of 1.0 Å over 35 Cα atoms, 1.2 Å over 37 Cα atoms, 2.6 Å over 103 Cα atoms, 2.6 Å over 124 Cα atoms for a single protomer of ORFV, respectively, and rmsd values of 1.1 Å over 70 Cα atoms, 1.2 Å over 74 Cα atoms, 2.6 Å over 206 Cα atoms and 2.7 Å over 248 Cα atoms for the dimeric configuration of ORFV125, respectively.

The crystal structure of the ORFV125: Bax BH3 complex revealed that binding of the Bax BH3 motif peptide to ORFV125 occurs via the canonical hydrophobic ligand-binding groove formed by helices α2–α5 (Figure 4a,b). Bax BH3 binding is mediated by a combination of ionic interactions, hydrogen bonds and hydrophobic interactions. Like other BH3-Bcl-2 interactions five hydrophobic residues of the Bax BH3 motif, L59, L63, I66, L70 and M74 engage the five hydrophobic pockets of the ORFV125 binding groove. In addition to the conserved hydrophobic interactions ionic interactions are formed between ORFV125 R86 and Bax D68 and ORFV125 E80 and Bax K64. These ionic interactions are supplemented by hydrogen bonding interaction between the main chain amide group of ORFV125 G87 and Bax D71 (Figure 4a). To identify local conformational changes in ORFV125 upon binding to Bax BH3 peptide we superimposed the Cα backbones of both *apo*-ORFV125 and the ORFV125: Bax BH3 complex. Upon Bax binding ORFV125 undergoes a conformational transformation where the C-terminal end of helix α3 is moving by 13.4 Å (Figure 4c) relative to its equivalent position in *apo*-ORFV. This is accompanied by a pivoting of the entire α3 helix allowing the α3 and α2 helices to form a contiguous α2 helix. In contrast, interactions of cellular Bcl-2, Bcl-x_L and Mcl-1 with Bax BH3 result in much smaller binding groove rearrangements, with observed shifts of the α3 helix by 7.3 Å, 8.3 Å and 3.3 Å, respectively. Notably, the regions corresponding to α3 of Bcl-2, Bcl-x_L or Mcl-1 in the ligand-free structures are largely unstructured, and adopt a more ordered helical structure upon ligand binding. *apo*-ORFV125, on the other hand features a fully ordered α3 helix that merges with α2 after Bax BH3 engagement. Amongst virus-encoded pro-survival Bcl-2 proteins, Epstein–Barr virus-encoded BHRF1 also displays a substantial ligand-binding groove rearrangement upon Bim BH3 binding (Figure 4d) [40,41]. However, these structural

Biochemical Journal (2020) **477** 4527–4541
https://doi.org/10.1042/BCJ20200776

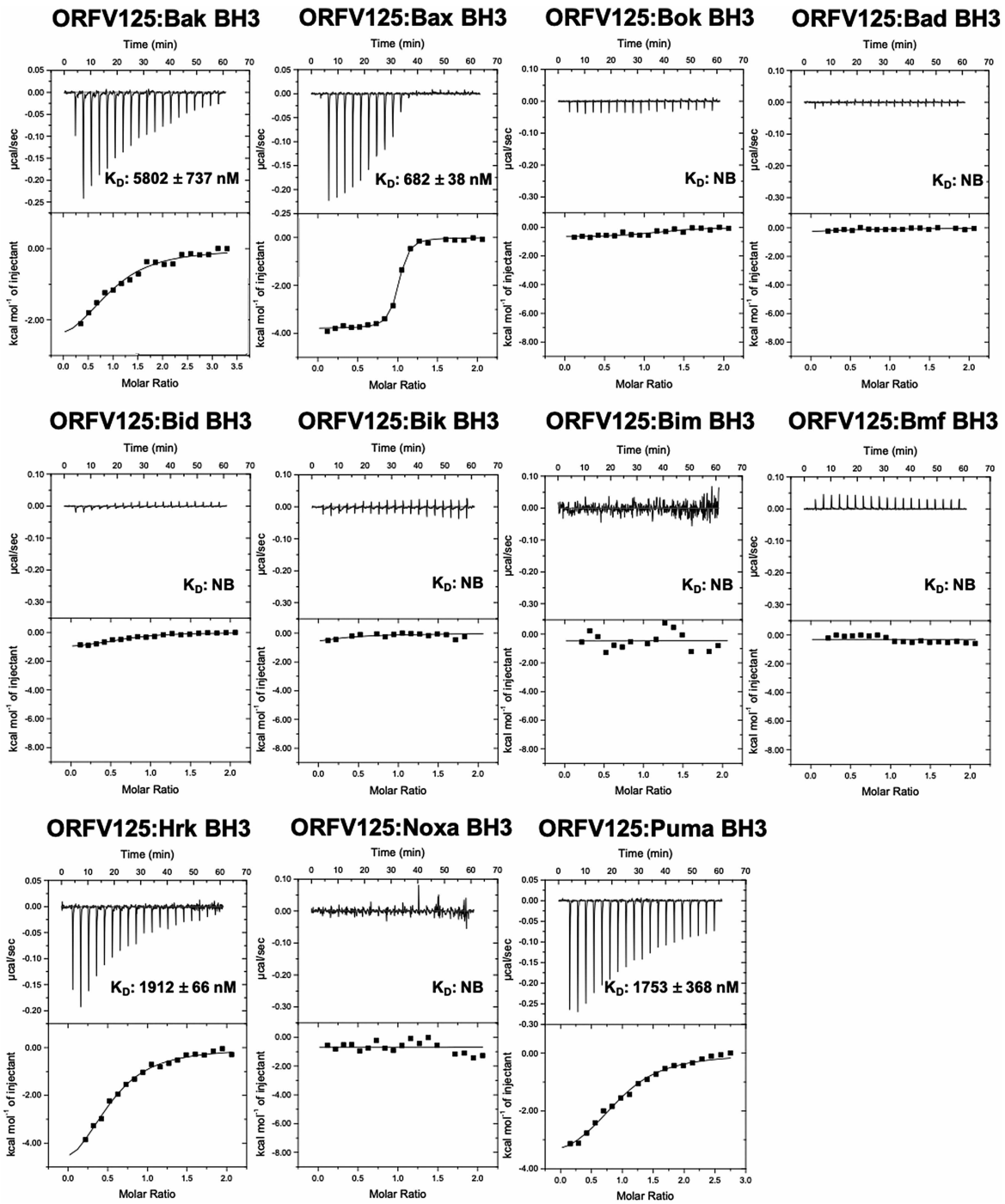

Figure 2. ORFV125 engages a range of BH3 motif peptides of pro-apoptotic Bcl-2 proteins.

Affinities of recombinant ORFV125 for BH3 motif peptides (26-mers, except for a Bid 34-mer and Bax 28-mers) were measured using ITC and the raw thermograms shown. K_D values (in nM) are the means of 3 experiments ± SD NB: no binding detected. The binding affinities are tabulated in Table 1.

changes centre on helix α4, which in this case rotates outwards to enlarge the binding groove. Amongst the *poxviridae*, only structures of myxomavirus M11L have been determined in both ligand-free and ligand-bound states. In contrast with ORFV125, structural changes upon ligand binding are minimal, with a 1.0 Å rmsd difference across the entire protein (Figure 4e) [42] when comparing the apo and holo forms of ORFV125.

Biochemical Journal (2020) **477** 4527–4541
https://doi.org/10.1042/BCJ20200776

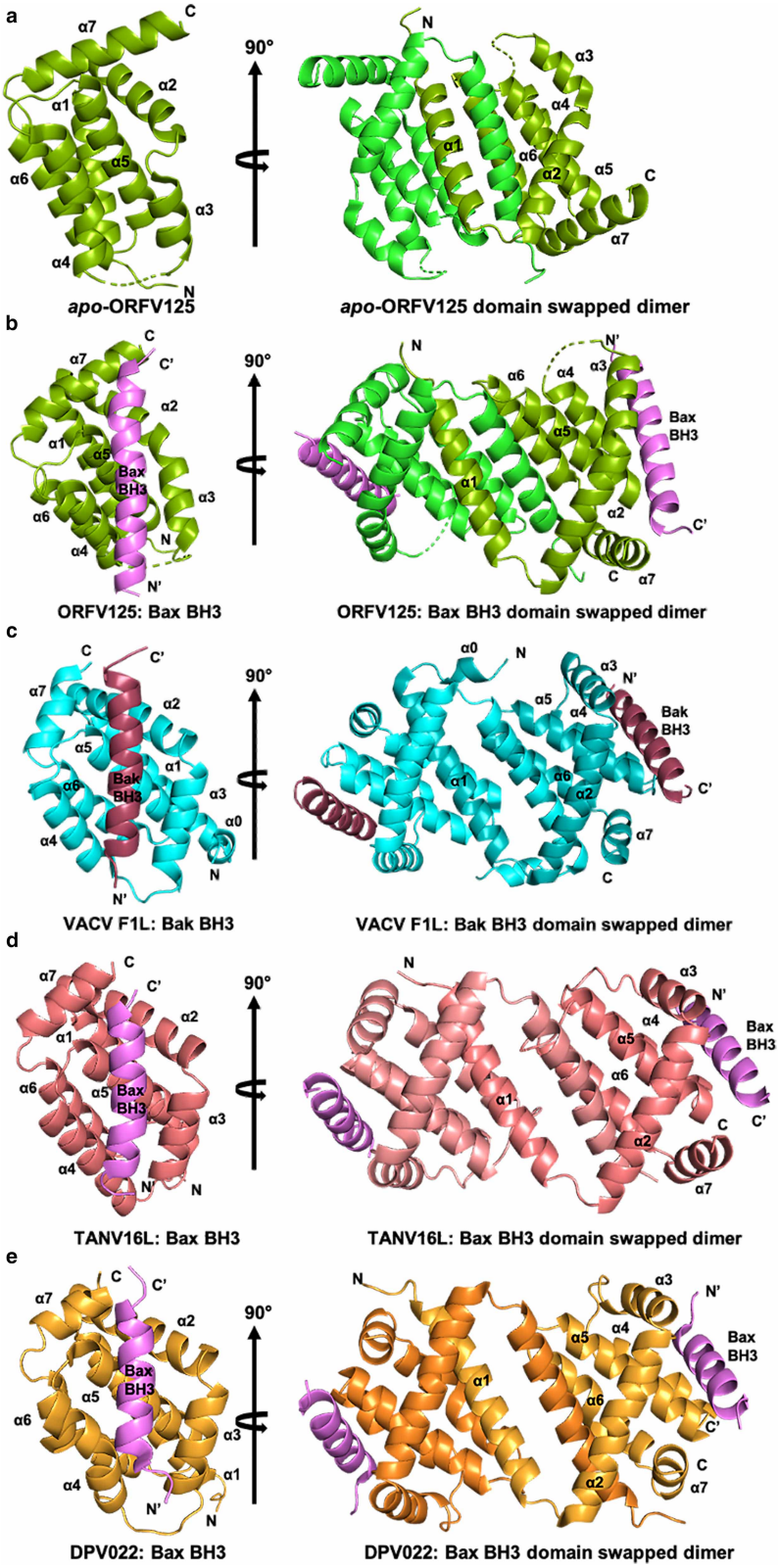

Figure 3. Cartoon representation of *apo*-ORFV125 and ORFV125 bound to Bax BH3 domain and comparison with other vBcl-2 dimeric structures. Part 1 of 2

(**a**) Structure of *apo*-ORFV125 (green). ORFV125 helices are labelled α1–α7. The view on the left in (a) is into the hydrophobic

Biochemical Journal (2020) **477** 4527–4541
https://doi.org/10.1042/BCJ20200776

Figure 3. Cartoon representation of *apo*-ORFV125 and ORFV125 bound to Bax BH3 domain and comparison with other vBcl-2 dimeric structures. Part 2 of 2

binding groove formed by helices α2–α5. On the right, the view is down the 2-fold symmetry axis between the domain-swapped α1 helices. (**b**) ORFV125 (green) in complex with the Bax BH3 peptide (magenta). (**c**) VACV F1L (cyan) in complex with the Bak BH3 domain (raspberry) [36]. (**d**) TANV16L (salmon) in complex with the Bax BH3 domain (magenta) [38] (**e**) DPV022 (gold) in complex with the Bax BH3 domain (magenta) [39]. The views in (**b–d**) are as in (**a**). In all cases, the view on the left is a single protomer and the right hand view the dimer.

To further validate the dimeric nature of ORFV125, we performed analytical size-exclusion chromatography (Figure 5) and compared recombinant ORFV125 with known molecular mass protein standards. Our results showed that ORFV125 eluted as a single peak in volume corresponding with dimeric assembly, supporting the dimeric structure of ORFV125 observed in our crystals.

Table 2. X-ray diffraction data collection and refinement statistics

	SeMet ORFV125: Bax BH3	ORFV125: Bax BH3 Native	*apo*-ORFV125 Native
Data collection			
Space group	C2	I2	$P6_222$
Cell dimensions			
a, *b*, *c* (Å)	109.37, 45.55, 69.35	69.51, 45.56, 105.96	106.61, 106.61, 60.58
α, *β*, *γ* (°)	90, 111.10, 90	90.00, 106.05, 90.00	90, 90, 120
Wavelength (Å)	0.9771	0.9537	0.9537
Resolution (Å)	49.69–2.52 (2.62–2.52)[1]	34.34–2.21 (2.28–2.21)[1]	50.66–2.22 (2.3–2.22)[1]
R_{sym} or R_{merge}	0.14 (0.99)	0.098 (0.59)	0.10 (2.21)
$I/\sigma I$	7.4 (1.2)	4.8 (1.0)	14.2 (1.2)
Completeness (%)	99.8 (99.2)	99.9 (99.6)	100 (100)
$CC_{1/2}$	0.99 (0.75)	0.99 (0.45)	1.0 (0.81)
Redundancy	6.9 (6.9)	3.5 (3.3)	19.2 (19.6)
Refinement			
Resolution (Å)		34.34–2.21 (2.28–2.21)	50.66–2.22 (2.3–2.22)
No. reflections		16 204	10 487
R_{work}/R_{free}		0.23/0.25	0.24/0.26
Clashscore		1.02	0.93
No. atoms			
Protein		2388	1043
Ligand/ion		81	39
Water		41	27
B-factors			
Protein		60.38	75.59
Ligand/ion		83.45	107.17
Water		63.47	82.29
Rms deviations			
Bond lengths (Å)		0.002	0.003
Bond angles (°)		0.50	0.55

[1]Values in parentheses are for the highest resolution shell.

Biochemical Journal (2020) **477** 4527–4541
https://doi.org/10.1042/BCJ20200776

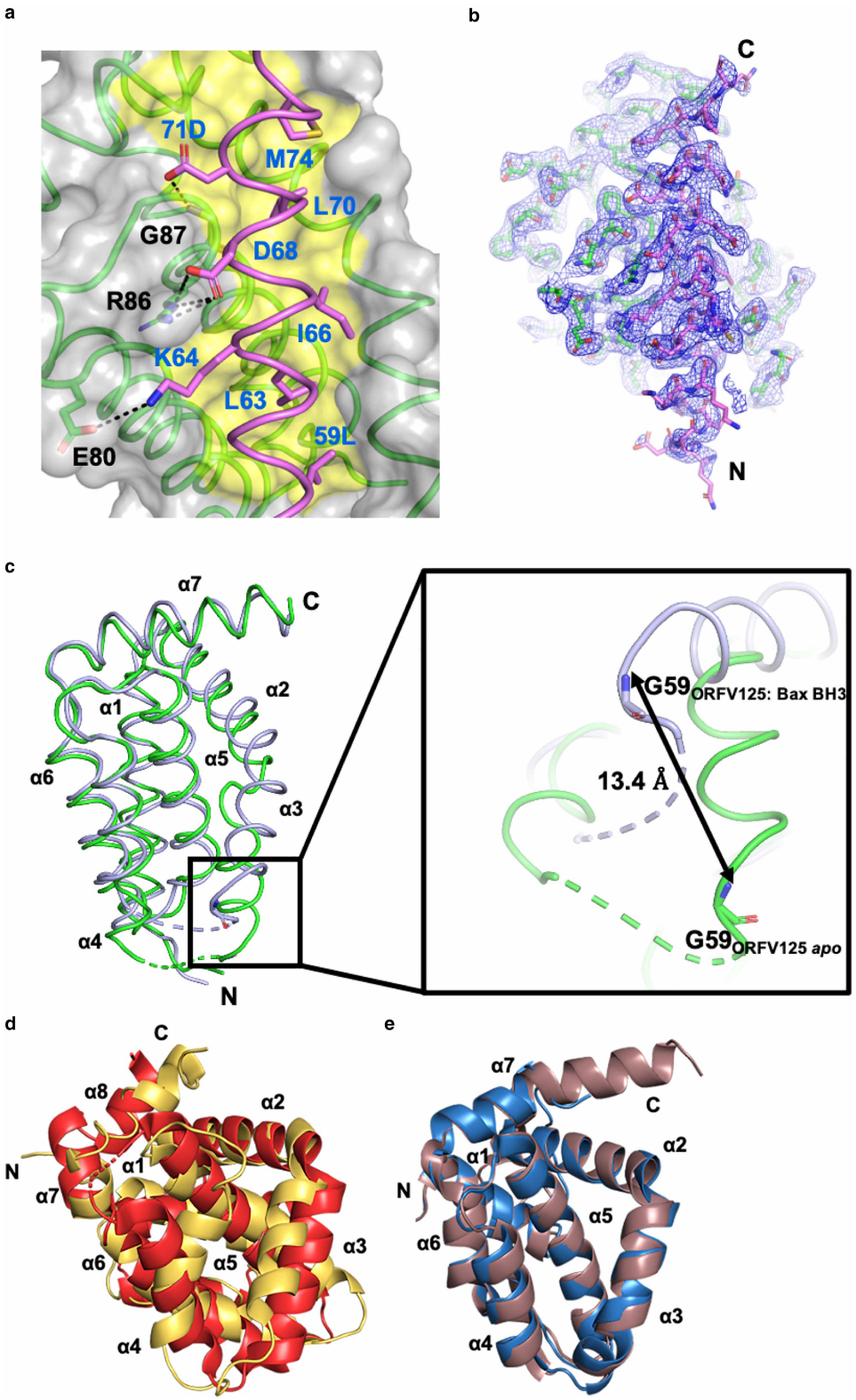

Figure 4. Detailed view of ORFV125 interactions with Bax BH3. Part 1 of 2

(**a**) Detailed view of the ORFV125: Bax BH3 interface. The ORFV125 surface, backbone and binding groove are shown in grey, green and yellow, respectively, while Bax BH3 is shown in magenta. The principle interacting residues of BaxBH3 are labelled in blue and those of ORFV125 in black. (**b**) 2Fo-Fc electron density map of ORFV125: Bax BH3 contoured at 1.5 σ. (**c**)

Biochemical Journal (2020) **477** 4527–4541
https://doi.org/10.1042/BCJ20200776

Figure 4. Detailed view of ORFV125 interactions with Bax BH3. Part 2 of 2

Superimposition of the protein Cα backbone of *apo*-ORFV (green) and ORFV of the ORFV125: Bax BH3 complex with the Bax BH3 peptide removed (grey). The inset shows an enlarged view of the protein backbone movement of the ORFV125 ligand-binding groove upon binding to Bax BH3 peptide. (**d**) A cartoon representation of *apo*-BHRF1 (PDB ID 1Q59) is shown in yellow, BHRF1:Bim BH3 (PDB ID 2WH6) is shown in red. (**e**) A cartoon representation of *apo*-M11L (PDB ID 2JBX) is shown in chocolate, M11L:Bak BH3 (PDB ID 2JBY) is shown in sky blue.

Analysis of interactions between pro-survival and the BH3-peptides of pro-apoptotic Bcl-2 proteins revealed that the conserved 'NWGR' sequence motif of BH1 region at the N-terminal end of the α5 helix (Figure 1) plays a pivotal role in the recognition of BH3-only proteins [43]. However, this conserved 'NWGR' motif is replaced by a 'SPGR' in the ORFV125 sequence but the key Gly and Arg residues remain conserved (Figure 1). This conserved Arg residue (R87) is involved in an ionic interaction with the highly conserved Asp (D68) residue of the Bax BH3 motif peptide and forms the hallmark interaction seen between mammalian pro-survival Bcl-2 proteins and BH3 motifs of pro-apoptotic Bcl-2 proteins [43]. The observation that despite the substitution of residues in the NWGR BH1 motif the Arg residue is still involved in a key ionic interaction mirrors observations from tanapox TANV16L [38] and sheeppox SPPV14 [44], where different Arg residues mimic the hallmark of ionic interactions observed in cellular Bcl-2 proteins and BH3 motif peptides of pro-apoptotic Bcl-2 proteins [4].

Discussion

Apoptosis is a powerful defence mechanism utilized by higher organisms against invading pathogens such as viruses [45]. However, viruses have evolved sophisticated strategies to hijack host cell suicide mechanisms to secure successful infection, subsequent replication and survival [3,46]. Several large DNA viruses encode Bcl-2 like genes that are vital virulence factors during early stage viral infections to counteract the host intrinsic apoptotic pathway and prevent premature host cell death [3]. ORFVs have been shown to bear many genes that interfere with host cell immune modulation but only a single gene ORF125 that directly inhibits the apoptotic

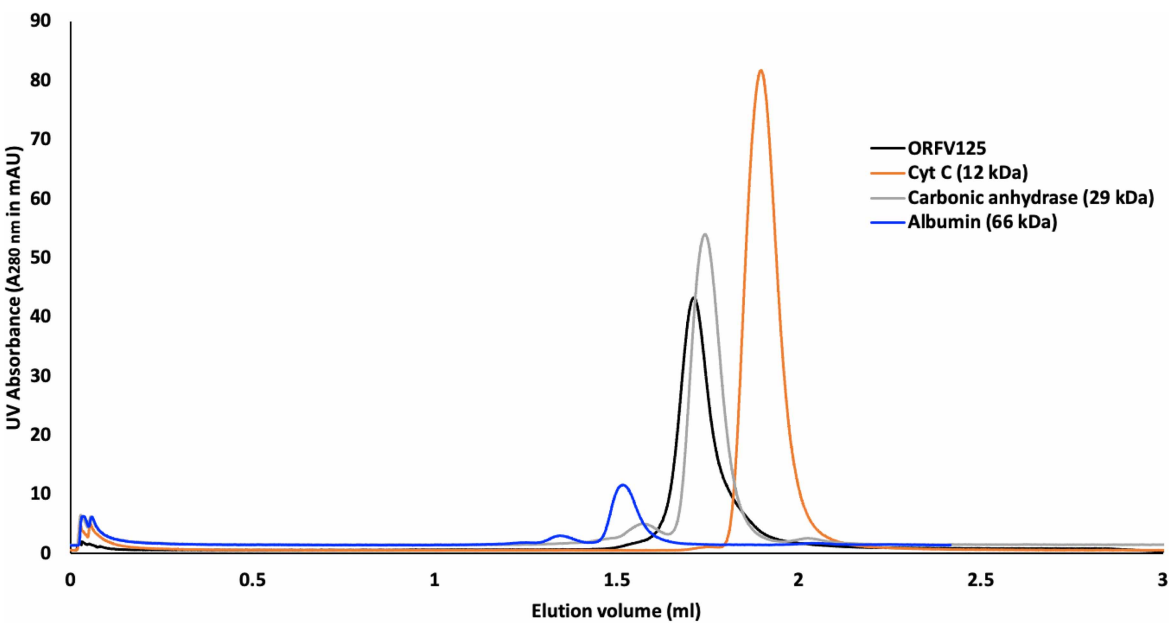

Figure 5. ORFV125 is a dimer in solution.

Size-exclusion chromatography of ORFV125 using a Superdex S75 3.2/300 column. The elution profile of the peak of interest (ORFV125) is 1.71 ml (black). The molecular mass standards shown are albumin (66 kDa) (blue), carbonic anhydrase (29 kDa) (grey) and cytochrome *c* (Cyt *c*) (12 kDa) (orange), AU: absorbance units at wavelength 280 nm.

response [20,47]. Remarkably, these viral Bcl-2 proteins may be highly sequence divergent from their host counterpart Bcl-2 homologues with no obvious shared sequence identity, including the BH motifs. Nevertheless, the common feature of these viral Bcl-2 proteins is that they resemble their mammalian counterparts by adopting the conserved α-helical Bcl-2 fold [40,42,44,48–52].

An earlier yeast two-hybrid screen found five potential interactors of ORFV125: cytochrome b, GUCY2C, BIRC5, GTF3C6 and SERBP1, but no follow-up binding experiments were performed on the purified protein [53]. In the present study, we report that ORFV125 interacts with a restricted subset of BH3 motif peptides from pro-apoptotic Bcl-2 proteins including those from Bax, Bak, Puma and Hrk (Table 1). The observed affinities are in the low nanomolar and micromolar range, unlike affinities measured for cellular pro-survival Bcl-2 proteins [54]. However, other domain-swapped viral Bcl-2 proteins [36–39] bind their interactors with comparable affinities to those seen for ORFV125. Intriguingly, ORFV125 did not bind the BH3 motif of Bim, a BH3-only protein considered the universal interactor for all previously reported cellular or viral pro-survival Bcl-2 proteins [55] except VARV F1L [37]. In contrast, previously reported evidence of BH3 interactions of ORFV125 by immunoprecipitation experiments showed that ORFV125 interacted with cellular Bim and Bik in addition to Bax, Puma and Hrk, but not with Bak [20]. Considering the impact of detergents on immunoprecipitation results [56] as well as the structure of Bcl-2 family proteins [13] the observation of differences between reported immunoprecipitation results and our affinity measurements are not entirely unexpected. Previously reported immunoprecipitation experiments were performed with full-length proteins transiently expressed in 293EBNA cells, whereas experiments reported here determined the binding of peptides spanning only the BH3 motif region of pro-apoptotic Bcl-2 proteins, which has been shown to recapitulate interactions between mammalian pro-survival and pro-apoptotic Bcl-2 protein [54] and is often in good agreement with immunoprecipitation results [40,42,57].

With certain cellular [58] and viral pro-survival Bcl-2 proteins [59,60] reported to modulate autophagy via their ability to bind Beclin-1, we also examined if ORFV125 harboured Beclin-1 affinity. However, no binding to Beclin-1 BH3 was observed, suggesting that ORFV125 does not feature broader cell death inhibitory activity beyond the intrinsic apoptosis pathway as seen in other pro-survival Bcl-2 proteins such as Bcl-x_L or A179L.

To investigate the structural basis for this restricted binding profile of ORFV125, we determined the crystal structures of ORFV125 on its own and in complex with highest affinity ligand, Bax BH3 motif peptide. Our analysis showed that ORFV125 adopts a domain-swapped dimeric Bcl-2 topology (Figure 3a,b) with conserved canonical Bcl-2 binding groove formed by α2–α5 as previously seen in other poxvirus Bcl-2 proteins VACV F1L, VARV F1L, TANV16L and DPV022 [36–39]. Whilst tanapox virus-encoded TANV16L existed both in a monomeric and domain-swapped dimeric Bcl-2 configuration in solution [38], ORFV125 exists only in a domain-swapped dimeric topology and we were unable to detect any other oligomeric state (Figure 5). This may suggest that the α1 helical component of ORFV125 is less flexible compared with that in TANV16L and thus not readily able to change position. Superimposition of the ORFV125 domain-swapped dimer with previously observed domain-swapped dimers from other poxviruses Bcl-2 proteins yields low rmsd values of less than 1.6 Å whilst TANV16L yields an rmsd of 3.3 Å, due to small variations in the length of helices and their overall arrangement. This may suggest that the arrangement of secondary structure elements is highly conserved among domain-swapped vBcl-2 proteins from the different poxviruses and that formation of these dimers may not allow for significant levels of variation to its fold.

Despite having a near-identical domain-swapped dimeric fold poxvirus encoded Bcl-2 proteins there are significant differences in their BH3 binding profiles (Figure 6). Compared with BH3 binding profiles of poxvirus encoded monomeric Bcl-2 proteins, myxoma virus M11L [42], sheeppox virus SPPV14 [44,51], fowlpox virus FPV039 [49] and canarypox virus CNP058 [61], domain-swapped dimeric Bcl-2 proteins show highly specific BH3 motif interactions and often bind only a few BH3 motif peptides with lower affinities. For instance, VACV F1L is only able to bind to Bim (K_D = 250 nM), Bak (K_D = 4300 nM) and Bax BH3 peptides (K_D = 1850 nM) (Figure 6b) [50] and functionally replaces Mcl-1 [62] and neutralizes Bim [36]. In contrast, VARV F1L binds Bak (K_D = 2640 nM), Bax (K_D = 960 nM) and Bid (K_D = 3200 nM) but not to Bim (Figure 6c) [37], and functionally VARV F1L only inhibits Bax but not Bak modulated apoptosis [37]. Similar to VACV F1L, DPV022 interact only with Bim (K_D = 340 nM), Bak (K_D = 6930 nM) and Bax (K_D = 4040 nM) (Figure 6e) [39] and functionally inhibits Bax and Bak regulated apoptosis [63]. While TANV16L displayed a broad spectrum of BH3 interactions compared with other domain-swapped dimeric poxvirus encoded Bcl-2 proteins and binds to almost all pro-apoptotic BH3 motif peptides except those of Noxa and Bok [38]. When considering the pro-apoptotic Bcl-2 interaction profile of ORFV125, the inability to bind Bim is striking, with ORFV125 only

Biochemical Journal (2020) **477** 4527–4541
https://doi.org/10.1042/BCJ20200776

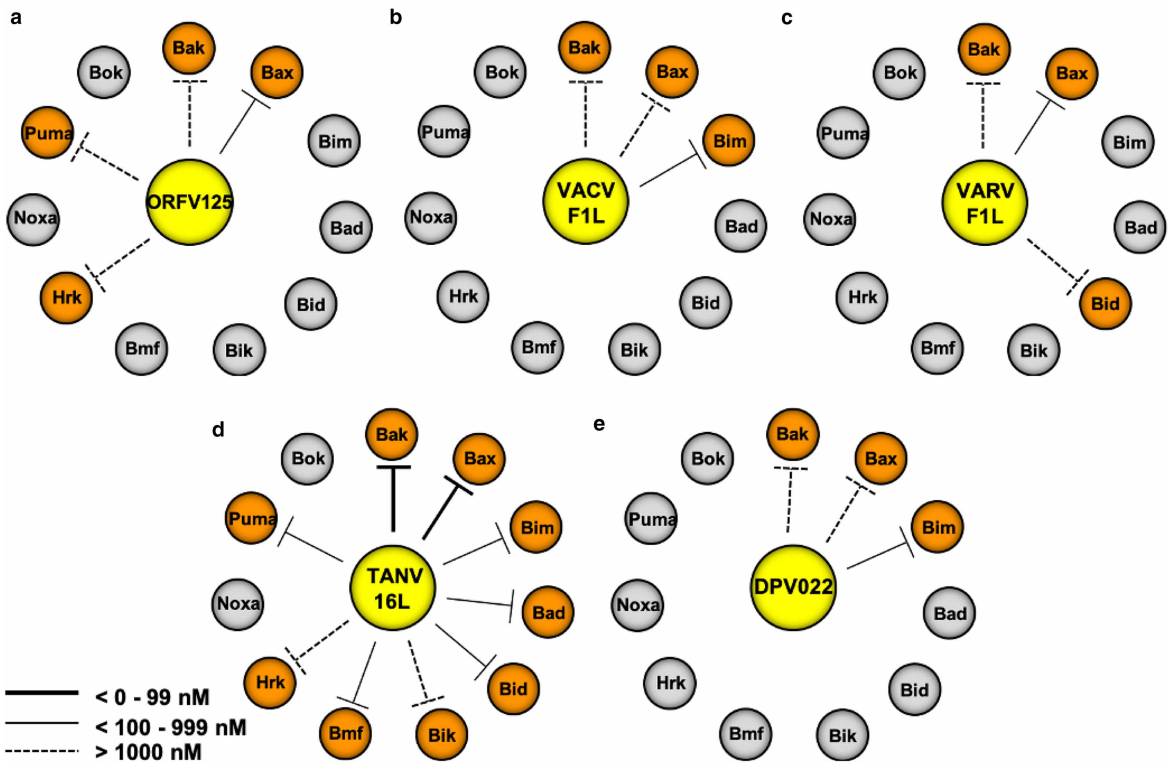

Figure 6. Comparison of the BH3 motif peptide binding profile of ORFV125 with other dimeric Bcl-2 homologues from other poxviruses.

Dimeric vBcl-2 proteins include vaccinia virus F1L (VACV F1L) (37), variola virus F1L (VARV F1L) [37], tanapox virus TANV16L [38], deerpox virus DPV022 [39]. (**a**) Binding profile of ORFV125 with BH3 motif peptides (**b**) binding profile of VACV F1L and (**c**) binding profile of VARV F1L, (**d**) binding profile of TANV16L and (**e**) binding profile of DPV022. The sequences of all BH3 motif peptides used in (**a**), (**b**) and (**c**) are of human origin. The line weight of the bars indicates the binding affinity ranges from 0 to 99 nM, <999 nM, and <1000 nM, as shown in the inset.

the second pro-survival Bcl-2 protein to not engage Bim, as is the inability to bind Noxa. Previous reports revealed that Bim and Noxa are up-regulated in human cells during ORFV infection [64] and Bak is up-regulated in sheep [65] and goat cells [66]. Furthermore, ORFV125 prevented both Bak and Bax induced apoptosis after UV irradiation. Altogether, this raises the possibility that it is primarily the ability to engage Bak and Bax that defines the pro-survival activity of ORFV125.

A comparison of previously predicted molecular contacts based on a suggested model for ORF125 [19] with our experimentally observed structures (Figure 4a) revealed substantial differences. The predicted structure for ORFV125 was based on a monomeric Bcl-2 fold, whereas in our hands ORFV125 exists as a dimer in solution as well as *in crystallo*. At the level of detailed interactions, S43, V47, L51, L55, V89, T90 and L94 were predicted to be involved in forming hydrophobic pockets. Our structures revealed that in addition, V42, L74, L78, G86, M98, L101, W102 and V136 also contribute to the formation of hydrophobic pockets in the binding groove. The conserved ionic interaction between $D99_{Bim}$ and $R87_{ORFV125}$ and the hydrogen bond interaction between $N102_{Bim}$ and $G86_{ORFV125}$ were predicted [19] and matched our crystal structure, whereas the additional salt bridge interaction between ORFV125 E80 and Bax K64 was not predicted. These findings indicate that the proposed structure of Westphal et al. [19] was of high quality in terms of predicting key conserved interactions, but failed to predict the domain-swap structure of homodimeric ORFV125.

In summary, we show that ORFV125 is a dimeric Bcl-2 protein with domain-swapped topology that is able to bind important host pro-apoptotic Bcl-2 members and potentially interfere with host cell apoptosis signalling in infected cells. Our findings provide a structural basis for dissecting the role of ORFV125 in ORFV infection and to define the contribution that suppression of Bcl-2 mediated apoptosis makes to the orf virus life

cycle. Such insights may be significant in the context of understanding the mechanism of ORFV125 regulation of apoptosis. Attenuated Orf viruses have been suggested as potential vectors for vaccine delivery as the virus only gives a short-lived immune response [67,68]. Consequently, understanding how orf immunomodulatory genes interact with human genes at a molecular level will aid in the design of safe and effective recombinant vector for orf virus-based vaccines.

Data Availability

Co-ordinate files have been deposited in the Protein Data Bank under the accession code 7ADS and 7ADT. All raw diffraction images were deposited on the SBGrid Data Bank using their PDB accession numbers.

Competing Interests

The authors declare that there are no competing interests associated with the manuscript.

Funding

This research was funded by La Trobe University (Scholarship to CDS).

CRediT Contribution

Marc Kvansakul: Conceptualization, Supervision, Funding acquisition, Investigation, Writing — original draft, Project administration, Writing — review and editing. **Chathura D. Suraweera**: Investigation, Writing — original draft, Writing — review and editing. **Mark G. Hinds**: Conceptualization, Supervision, Writing — original draft, Writing — review and editing.

Open Access

Open access for this article was enabled by the participation of La Trobe University in an all-inclusive *Read & Publish* pilot with Portland Press and the Biochemical Society under a transformative agreement with CAUL.

Acknowledgements

We thank staff at the MX beamlines at the Australian Synchrotron for help with X-ray data collection. This research was undertaken in part using the MX2 beamline at the Australian Synchrotron, part of ANSTO, and made use of the Australian Cancer Research Foundation (ACRF) detector. We thank the Comprehensive Proteomics Platform at La Trobe University for core instrument support.

Abbreviations

Bcl-2, B-cell lymphoma 2; BH, Bcl-2 homology; ITC, isothermal titration calorimetry.

References

1 Jorgensen, I., Rayamajhi, M. and Miao, E.A. (2017) Programmed cell death as a defence against infection. *Nat. Rev. Immunol.* **17**, 151–164 https://doi.org/10.1038/nri.2016.147
2 Benedict, C.A., Norris, P.S. and Ware, C.F. (2002) To kill or be killed: viral evasion of apoptosis. *Nat. Immunol.* **3**, 1013–1018 https://doi.org/10.1038/ni1102-1013
3 Kvansakul, M., Caria, S. and Hinds, M.G. (2017) The Bcl-2 family in host-virus interactions. *Viruses* **9**, 290 https://doi.org/10.3390/v9100290
4 Banjara, S., Suraweera, C.D., Hinds, M.G. and Kvansakul, M. (2020) The Bcl-2 family: ancient origins, conserved structures, and divergent mechanisms. *Biomolecules* **10**, 128 https://doi.org/10.3390/biom10010128
5 Tait, S.W. and Green, D.R. (2013) Mitochondrial regulation of cell death. *Cold Spring Harb. Perspect. Biol.* **5**, a008706 https://doi.org/10.1101/cshperspect.a008706
6 Youle, R.J. and Strasser, A. (2008) The BCL-2 protein family: opposing activities that mediate cell death. *Nat. Rev. Mol. Cell Biol.* **9**, 47–59 https://doi.org/10.1038/nrm2308
7 Petros, A.M., Olejniczak, E.T. and Fesik, S.W. (2004) Structural biology of the Bcl-2 family of proteins. *Biochim. Biophys. Acta* **1644**, 83–94 https://doi.org/10.1016/j.bbamcr.2003.08.012
8 Kvansakul, M. and Hinds, M.G. (2013) Structural biology of the Bcl-2 family and its mimicry by viral proteins. *Cell Death Disease* **4**, e909-e https://doi.org/10.1038/cddis.2013.436
9 Kvansakul, M. and Hinds, M.G. (2014) The structural biology of BH3-only proteins. *Methods Enzymol.* **544**, 49–74 https://doi.org/10.1016/B978-0-12-417158-9.00003-0
10 Luo, X., O'Neill, K.L. and Huang, K. (2020) The third model of Bax/Bak activation: a Bcl-2 family feud finally resolved? *F1000Res* **9**, 935 https://doi.org/10.12688/f1000research.25607.1
11 Shamas-Din, A., Kale, J., Leber, B. and Andrews, D.W. (2013) Mechanisms of action of Bcl-2 family proteins. *Cold Spring Harb. Perspect. Biol.* **5**, a008714 https://doi.org/10.1101/cshperspect.a008714

Biochemical Journal (2020) **477** 4527–4541
https://doi.org/10.1042/BCJ20200776

12 Kvansakul, M. and Hinds, M.G. (2015) The Bcl-2 family: structures, interactions and targets for drug discovery. *Apoptosis* **20**, 136–150 https://doi.org/10.1007/s10495-014-1051-7
13 Czabotar, P.E., Westphal, D., Dewson, G., Ma, S., Hockings, C., Fairlie, W.D. et al. (2013) Bax crystal structures reveal how BH3 domains activate Bax and nucleate its oligomerization to induce apoptosis. *Cell* **152**, 519–531 https://doi.org/10.1016/j.cell.2012.12.031
14 McArthur, K., Whitehead, L.W., Heddleston, J.M., Li, L., Padman, B.S., Oorschot, V. et al. (2018) BAK/BAX macropores facilitate mitochondrial herniation and mtDNA efflux during apoptosis. *Science* **359**, eaao6047 https://doi.org/10.1126/science.aao6047
15 Dorstyn, L., Akey, C.W. and Kumar, S. (2018) New insights into apoptosome structure and function. *Cell Death Differ.* **25**, 1194–1208 https://doi.org/10.1038/s41418-017-0025-z
16 Neumann, S., El Maadidi, S., Faletti, L., Haun, F., Labib, S., Schejtman, A. et al. (2015) How do viruses control mitochondria-mediated apoptosis? *Virus Res.* **209**, 45–55 https://doi.org/10.1016/j.virusres.2015.02.026
17 Fleming, S.B. and Mercer, A.A. (2007) Genus parapoxvirus. In *Poxviruses* (Mercer, A.A., Schmidt, A. and Weber, O., eds), pp. 127–165 https://doi.org/10.1007/978-3-7643-7557-7_7
18 Ginzburg, V.E. and Liauchonak, I. (2017) Human orf: atypical rash in an urban medical practice. *Can. Fam. Physician.* **63**, 769–771 PMID: 29025803
19 Westphal, D., Ledgerwood, E.C., Hibma, M.H., Fleming, S.B., Whelan, E.M. and Mercer, A.A. (2007) A novel Bcl-2-like inhibitor of apoptosis is encoded by the parapoxvirus orf virus. *J. Virol.* **81**, 7178 https://doi.org/10.1128/JVI.00404-07
20 Westphal, D., Ledgerwood, E.C., Tyndall, J.D., Hibma, M.H., Ueda, N., Fleming, S.B. et al. (2009) The orf virus inhibitor of apoptosis functions in a Bcl-2-like manner, binding and neutralizing a set of BH3-only proteins and active Bax. *Apoptosis* **14**, 1317–1330 https://doi.org/10.1007/s10495-009-0403-1
21 Guerrero, S.A., Hecht, H.J., Hofmann, B., Biebl, H. and Singh, M. (2001) Production of selenomethionine-labelled proteins using simplified culture conditions and generally applicable host/vector systems. *Appl. Microbiol. Biotechnol.* **56**, 718–723 https://doi.org/10.1007/s002530100690
22 Caria, S., Hinds, M.G. and Kvansakul, M. (2017) Structural insight into an evolutionarily ancient programmed cell death regulator - the crystal structure of marine sponge BHP2 bound to LB-Bak-2. *Cell Death Dis.* **8**, e2543 https://doi.org/10.1038/cddis.2016.469
23 Kvansakul, M. and Czabotar, P.E. (2016) Preparing samples for crystallization of Bcl-2 family complexes. *Methods Mol. Biol.* **1419**, 213–229 https://doi.org/10.1007/978-1-4939-3581-9_16
24 Aragão, D., Aishima, J., Cherukuvada, H., Clarken, R., Clift, M., Cowieson, N.P., et al. (2018) MX2: a high-flux undulator microfocus beamline serving both the chemical and macromolecular crystallography communities at the Australian synchrotron. *J. Synchrotron. Radiat.* **25**(Pt 3), 885–891 https://doi.org/10.1107/S1600577518003120
25 Kabsch, W. (2010) XDS. *Acta Crystallogr. D Biol. Crystallogr.* **66**(Pt 2), 125–132 https://doi.org/10.1107/S0907444909047337
26 Evans, P. (2006) Scaling and assessment of data quality. *Acta Crystallogr. D Biol. Crystallogr.* **62**(Pt1), 72–82 https://doi.org/10.1107/S0907444905036693
27 Cowieson, N.P., Aragao, D., Clift, M., Ericsson, D.J., Gee, C., Harrop, S.J. et al. (2015) MX1: a bending-magnet crystallography beamline serving both chemical and macromolecular crystallography communities at the Australian synchrotron. *J. Synchrotron Radiat.* **22**, 187–190 https://doi.org/10.1107/S1600577514021717
28 Sheldrick, G.M. (2010) Experimental phasing with SHELXC/D/E: combining chain tracing with density modification. *Acta Crystallogr. D Biol. Crystallogr.* **66**(Pt 4), 479–485 https://doi.org/10.1107/S0907444909038360
29 Afonine, P.V., Grosse-Kunstleve, R.W., Echols, N., Headd, J.J., Moriarty, N.W., Mustyakimov, M., et al. (2012) Towards automated crystallographic structure refinement with phenix.refine. *Acta Crystallogr. D Biol. Crystallogr.* **68**(Pt 4), 352–367 https://doi.org/10.1107/S0907444912001308
30 Terwilliger, T.C., Grosse-Kunstleve, R.W., Afonine, P.V., Moriarty, N.W., Zwart, P.H., Hung, L.W., et al. (2008) Iterative model building, structure refinement and density modification with the PHENIX autoBuild wizard. *Acta Crystallogr. D Biol. Crystallogr.* **64**(Pt 1), 61–69 https://doi.org/10.1107/S090744490705024X
31 McCoy, A.J. (2007) Solving structures of protein complexes by molecular replacement with phaser. *Acta Crystallogr. D Biol. Crystallogr.* **63**(Pt 1), 32–41 https://doi.org/10.1107/S0907444906045975
32 Emsley, P., Lohkamp, B., Scott, W.G. and Cowtan, K. (2010) Features and development of coot. *Acta Crystallogr. D Biol. Crystallogr.* **66**(Pt 4), 486–501 https://doi.org/10.1107/S0907444910007493
33 Morin, A., Eisenbraun, B., Key, J., Sanschagrin, P.C., Timony, M.A., Ottaviano, M. et al. (2013) Collaboration gets the most out of software. *eLife* **2**, e01456 https://doi.org/10.7554/eLife.01456
34 Meyer, P.A., Socias, S., Key, J., Ransey, E., Tjon, E.C., Buschiazzo, A. et al. (2016) Data publication with the structural biology data grid supports live analysis. *Nat. Commun.* **7**, 10882 https://doi.org/10.1038/ncomms10882
35 Edgar, R.C. (2004) MUSCLE: a multiple sequence alignment method with reduced time and space complexity. *BMC Bioinform.* **5**, 113 https://doi.org/10.1186/1471-2105-5-113
36 Campbell, S., Thibault, J., Mehta, N., Colman, P.M., Barry, M. and Kvansakul, M. (2014) Structural insight into BH3 domain binding of vaccinia virus antiapoptotic F1L. *J. Virol.* **88**, 8667 https://doi.org/10.1128/JVI.01092-14
37 Marshall, B., Puthalakath, H., Caria, S., Chugh, S., Doerflinger, M., Colman, P.M. et al. (2015) Variola virus F1L is a Bcl-2-like protein that unlike its vaccinia virus counterpart inhibits apoptosis independent of Bim. *Cell Death Dis.* **6**, e1680-e https://doi.org/10.1038/cddis.2015.52
38 Suraweera, C.D., Anasir, M.I., Chugh, S., Javorsky, A., Impey, R.E., Hasan Zadeh, M. et al. (2020) Structural insight into tanapoxvirus-mediated inhibition of apoptosis. *FEBS J.* **287**, 3733–3750 https://doi.org/10.1111/febs.15365
39 Burton, D.R., Caria, S., Marshall, B., Barry, M. and Kvansakul, M. (2015) Structural basis of deerpox virus-mediated inhibition of apoptosis. *Acta Crystallogr. D Biol. Crystallogr.* **71**(Pt 8), 1593–1603 https://doi.org/10.1107/S1399004715009402
40 Kvansakul, M., Wei, A.H., Fletcher, J.I., Willis, S.N., Chen, L., Roberts, A.W. et al. (2010) Structural basis for apoptosis inhibition by Epstein–Barr virus BHRF1. *PLoS Pathog.* **6**, e1001236 https://doi.org/10.1371/journal.ppat.1001236
41 Huang, Q., Petros, A.M., Virgin, H.W., Fesik, S.W. and Olejniczak, E.T. (2003) Solution structure of the BHRF1 protein from Epstein–Barr virus, a homolog of human Bcl-2. *J. Mol. Biol.* **332**, 1123–1130 https://doi.org/10.1016/j.jmb.2003.08.007
42 Kvansakul, M., van Delft, M.F., Lee, E.F., Gulbis, J.M., Fairlie, W.D., Huang, D.C. et al. (2007) A structural viral mimic of prosurvival Bcl-2: a pivotal role for sequestering proapoptotic Bax and Bak. *Mol. Cell* **25**, 933–942 https://doi.org/10.1016/j.molcel.2007.02.004

43 Day, C.L., Smits, C., Fan, F.C., Lee, E.F., Fairlie, W.D. and Hinds, M.G. (2008) Structure of the BH3 domains from the p53-inducible BH3-only proteins Noxa and Puma in complex with Mcl-1. *J. Mol. Biol.* **380**, 958–971 https://doi.org/10.1016/j.jmb.2008.05.071
44 Suraweera, C.D., Burton, D.R., Hinds, M.G. and Kvansakul, M. (2020) Crystal structures of the sheeppox virus encoded inhibitor of apoptosis SPPV14 bound to the proapoptotic BH3 peptides Hrk and Bax. *FEBS Lett.* **594**, 2016–2026 https://doi.org/10.1002/1873-3468.13807
45 Fuchs, Y. and Steller, H. (2015) Live to die another way: modes of programmed cell death and the signals emanating from dying cells. *Nat. Rev. Mol. Cell Biol.* **16**, 329–344 https://doi.org/10.1038/nrm3999
46 Galluzzi, L., Brenner, C., Morselli, E., Touat, Z. and Kroemer, G. (2008) Viral control of mitochondrial apoptosis. *PLoS Pathog.* **4**, e1000018 https://doi.org/10.1371/journal.ppat.1000018
47 Fleming, S.B., Wise, L.M. and Mercer, A.A. (2015) Molecular genetic analysis of orf virus: a poxvirus that has adapted to skin. *Viruses* **7**, 1505–1539 https://doi.org/10.3390/v7031505
48 Banjara, S., Caria, S., Dixon, L.K., Hinds, M.G. and Kvansakul, M. (2017) Structural insight into African swine fever virus A179L-mediated inhibition of apoptosis. *J. Virol.* **91**, e02228-16 https://doi.org/10.1128/JVI.02228-16
49 Anasir, M.I., Caria, S., Skinner, M.A. and Kvansakul, M. (2017) Structural basis of apoptosis inhibition by the fowlpox virus protein FPV039. *J. Biol. Chem.* **292**, 9010–9021 https://doi.org/10.1074/jbc.M116.768879
50 Kvansakul, M., Yang, H., Fairlie, W.D., Czabotar, P.E., Fischer, S.F., Perugini, M.A. et al. (2008) Vaccinia virus anti-apoptotic F1L is a novel Bcl-2-like domain-swapped dimer that binds a highly selective subset of BH3-containing death ligands. *Cell Death Differ.* **15**, 1564–1571 https://doi.org/10.1038/cdd.2008.83
51 Okamoto, T., Campbell, S., Mehta, N., Thibault, J., Colman, P.M., Barry, M. et al. (2012) Sheeppox virus SPPV14 encodes a Bcl-2-like cell death inhibitor that counters a distinct set of mammalian proapoptotic proteins. *J. Virol.* **86**, 11501–11511 https://doi.org/10.1128/JVI.01115-12
52 Banjara, S., Mao, J., Ryan, T.M., Caria, S. and Kvansakul, M. (2018) Grouper iridovirus GIV66 is a Bcl-2 protein that inhibits apoptosis by exclusively sequestering Bim. *J. Biol. Chem.* **293**, 5464–5477 https://doi.org/10.1074/jbc.RA117.000591
53 Tian, H., Chen, Y., Wu, J., Lin, T. and Liu, X. (2016) Identification and function analysis of the host cell protein that interacted with Orf virus Bcl-2-like protein ORFV125. *Res. Vet. Sci.* **108**, 93–97 https://doi.org/10.1016/j.rvsc.2016.08.005
54 Chen, L., Willis, S.N., Wei, A., Smith, B.J., Fletcher, J.I., Hinds, M.G. et al. (2005) Differential targeting of prosurvival Bcl-2 proteins by their BH3-only ligands allows complementary apoptotic function. *Mol. Cell* **17**, 393–403 https://doi.org/10.1016/j.molcel.2004.12.030
55 Rautureau, G.J., Yabal, M., Yang, H., Huang, D.C., Kvansakul, M. and Hinds, M.G. (2012) The restricted binding repertoire of Bcl-B leaves Bim as the universal BH3-only prosurvival Bcl-2 protein antagonist. *Cell Death Dis.* **3**, e443 https://doi.org/10.1038/cddis.2012.178
56 Hsu, Y.T. and Youle, R.J. (1997) Nonionic detergents induce dimerization among members of the Bcl-2 family. *J. Biol. Chem.* **272**, 13829–13834 https://doi.org/10.1074/jbc.272.21.13829
57 Popgeorgiev, N., Sa, J.D., Jabbour, L., Banjara, S., Nguyen, T.T.M., Akhavan-E-Sabet, A. et al. (2020) Ancient and conserved functional interplay between Bcl-2 family proteins in the mitochondrial pathway of apoptosis. *Sci. Adv.* **6**, eabc4149 https://doi.org/10.1126/sciadv.abc4149
58 Oberstein, A., Jeffrey, P.D. and Shi, Y. (2007) Crystal structure of the Bcl-XL-Beclin 1 peptide complex: Beclin 1 is a novel BH3-only protein. *J. Biol. Chem.* **282**, 13123–13132 https://doi.org/10.1074/jbc.M700492200
59 Banjara, S., Shimmon, G.L., Dixon, L.K., Netherton, C.L., Hinds, M.G. and Kvansakul, M. (2019) Crystal structure of African swine fever virus A179L with the autophagy regulator Beclin. *Viruses* **11**, 789 https://doi.org/10.3390/v11090789
60 Ku, B., Woo, J.S., Liang, C., Lee, K.H., Jung, J.U. and Oh, B.H. (2008) An insight into the mechanistic role of Beclin 1 and its inhibition by prosurvival Bcl-2 family proteins. *Autophagy* **4**, 519–520 https://doi.org/10.4161/auto.5846
61 Anasir, M.I., Baxter, A.A., Poon, I.K.H., Hulett, M.D. and Kvansakul, M. (2017) Structural and functional insight into canarypox virus CNP058 mediated regulation of apoptosis. *Viruses* **9**, 305 https://doi.org/10.3390/v9100305
62 Campbell, S., Hazes, B., Kvansakul, M., Colman, P. and Barry, M. (2010) Vaccinia virus F1L interacts with Bak using highly divergent Bcl-2 homology domains and replaces the function of Mcl-1. *J. Biol. Chem.* **285**, 4695–4708 https://doi.org/10.1074/jbc.M109.053769
63 Banadyga, L., Lam, S.C., Okamoto, T., Kvansakul, M., Huang, D.C. and Barry, M. (2011) Deerpox virus encodes an inhibitor of apoptosis that regulates Bak and Bax. *J. Virol.* **85**, 1922–1934 https://doi.org/10.1128/JVI.01959-10
64 Chen, D., Long, M., Xiao, B., Xiong, Y., Chen, H., Chen, Y. et al. (2017) Transcriptomic profiles of human foreskin fibroblast cells in response to orf virus. *Oncotarget* **8**, 58668–58685 https://doi.org/10.18632/oncotarget.17417
65 Jia, H., Zhan, L., Wang, X., He, X., Chen, G., Zhang, Y. et al. (2017) Transcriptome analysis of sheep oral mucosa response to Orf virus infection. *PLoS One* **12**, e0186681 https://doi.org/10.1371/journal.pone.0186681
66 Hao, J.H., Kong, H.J., Yan, M.H., Shen, C.C., Xu, G.W., Zhang, D.J. et al. (2020) Inhibition of orf virus replication in goat skin fibroblast cells by the HSPA1B protein, as demonstrated by iTRAQ-based quantitative proteome analysis. *Arch. Virol.* **165**, 2561–2587 https://doi.org/10.1007/s00705-020-04789-y
67 Reguzova, A., Ghosh, M., Muller, M., Rziha, H.J. and Amann, R. (2020) Orf virus-based vaccine vector D1701-V induces strong CD8+ T cell response against the transgene but not against ORFV-derived epitopes. *Vaccines (Basel)* **8**, 295 https://doi.org/10.3390/vaccines8020295
68 Wang, R., Wang, Y., Liu, F. and Luo, S. (2019) Orf virus: a promising new therapeutic agent. *Rev. Med. Virol.* **29**, e2013 https://doi.org/10.1002/rmv.2013

Mass Spectrum

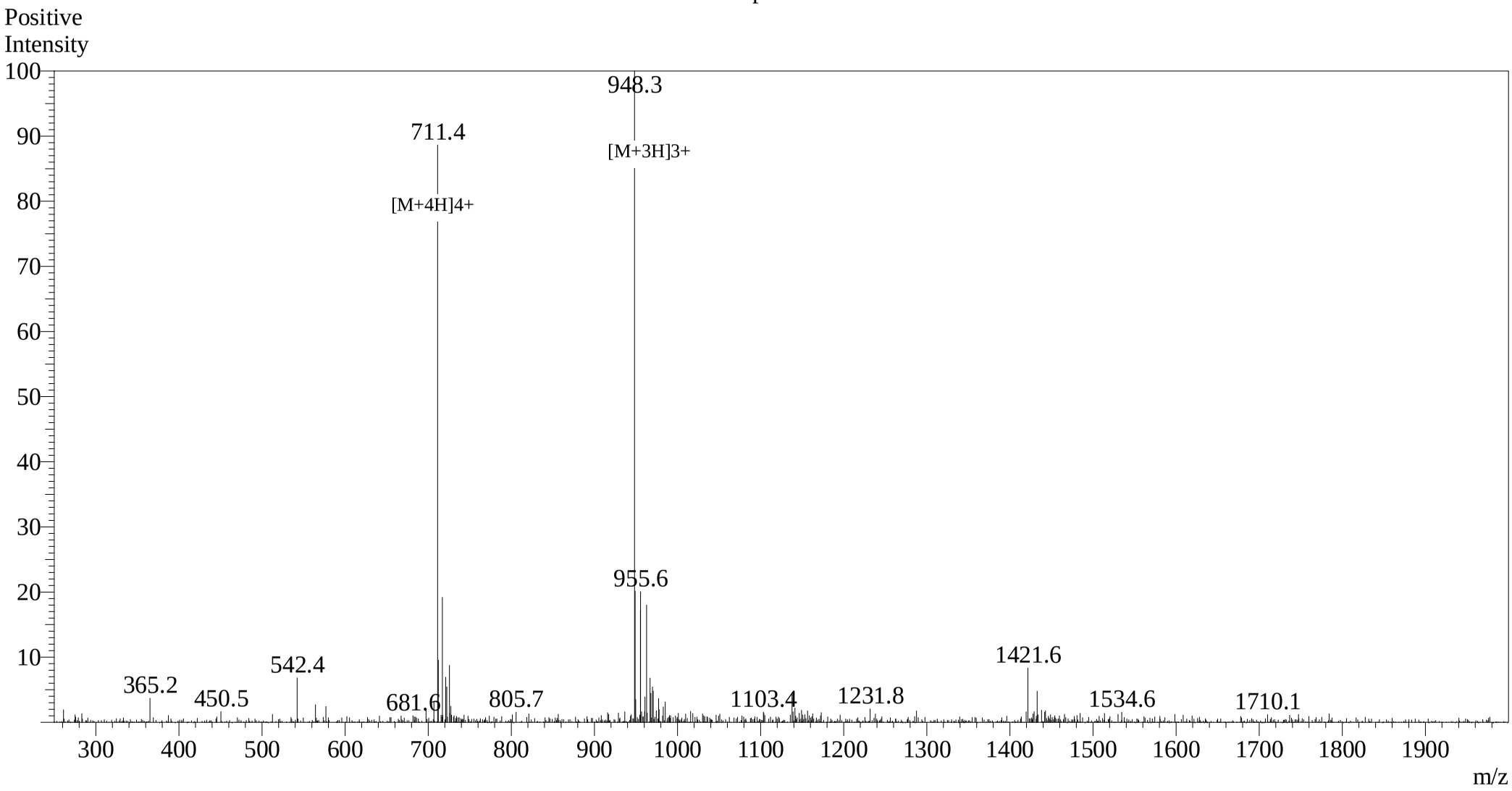

Sample Information

Acquired by :	Gary
Month-Day Processed :	11/28/19
Time Processed :	21:12:58
Injection Volume :	0.3
Sample Name :	hs_Beclin
Sample ID :	U4406EK070-1
Theoretical MW :	2842.18
Observed MW :	2841.9

Interface	:ESI
Nebulizing Gas Flow	:1.5L/min
CDL Temp	:250
Block Temp	:200

Equipment	: GK11010007
Interface Bias	: +4.5 kV
Drying Gas Flow	:5 L/min
T.Flow	:0.2 ml/min
B.conc	:50%H2O/50%MeOH

Mass Spectrum

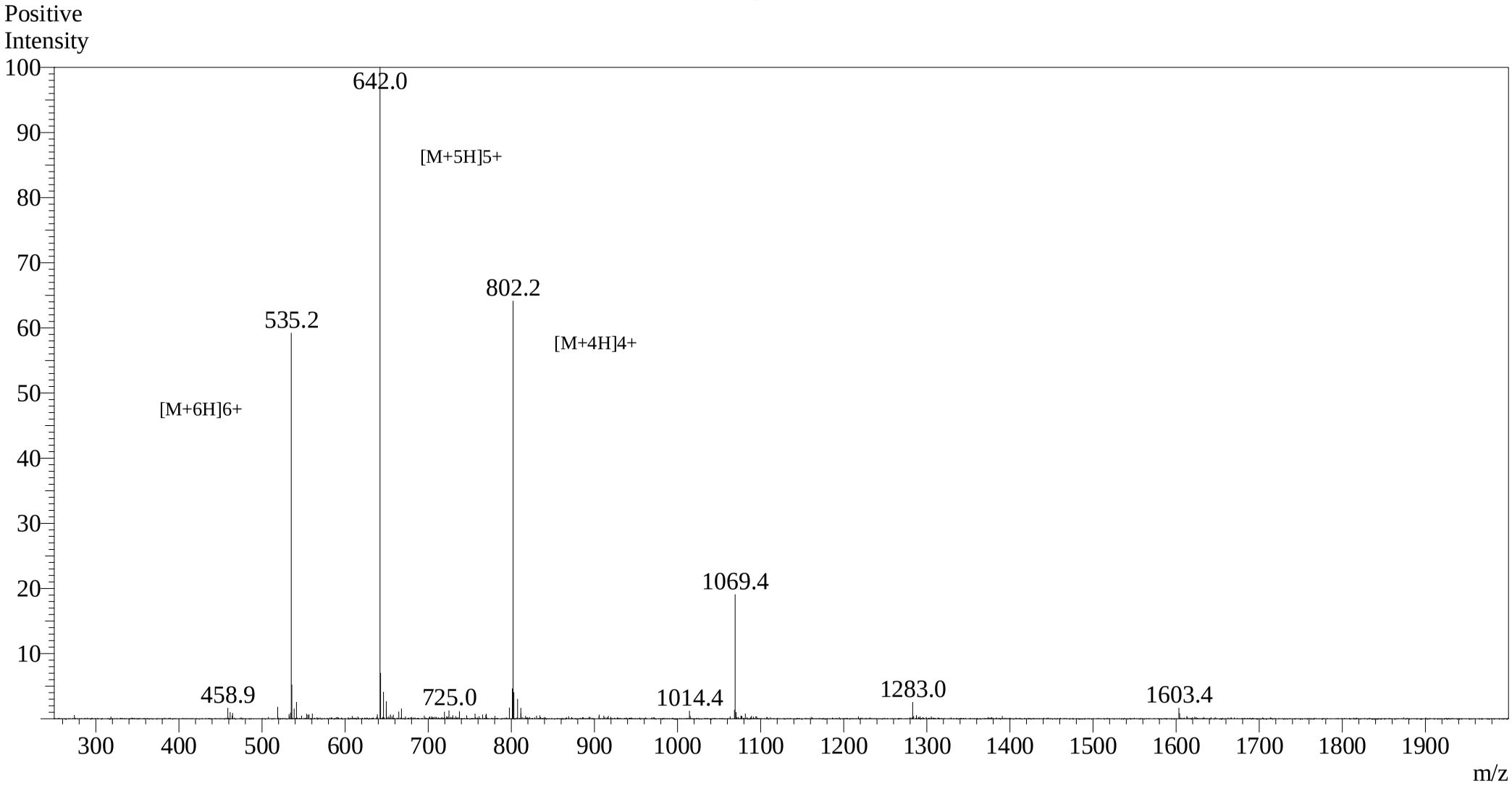

Sample Information

Acquired by :	Gary
Month-Day Processed :	03/24/20
Time Processed :	10:51:43
Injection Volume :	0.3
Sample Name :	HS_Puma
Sample ID :	U6608FC030-1
Theoretical MW :	3205.50
Observed MW :	3205.0

Interface	:ESI
Nebulizing Gas Flow	:1.5L/min
CDL Temp	:250
Block Temp	:200

Equipment	: GK11010007
Interface Bias	: +4.5 kV
Drying Gas Flow	:5 L/min
T.Flow	:0.2 ml/min
B.conc	:50%H2O/50%MeOH

Mass Spectrum

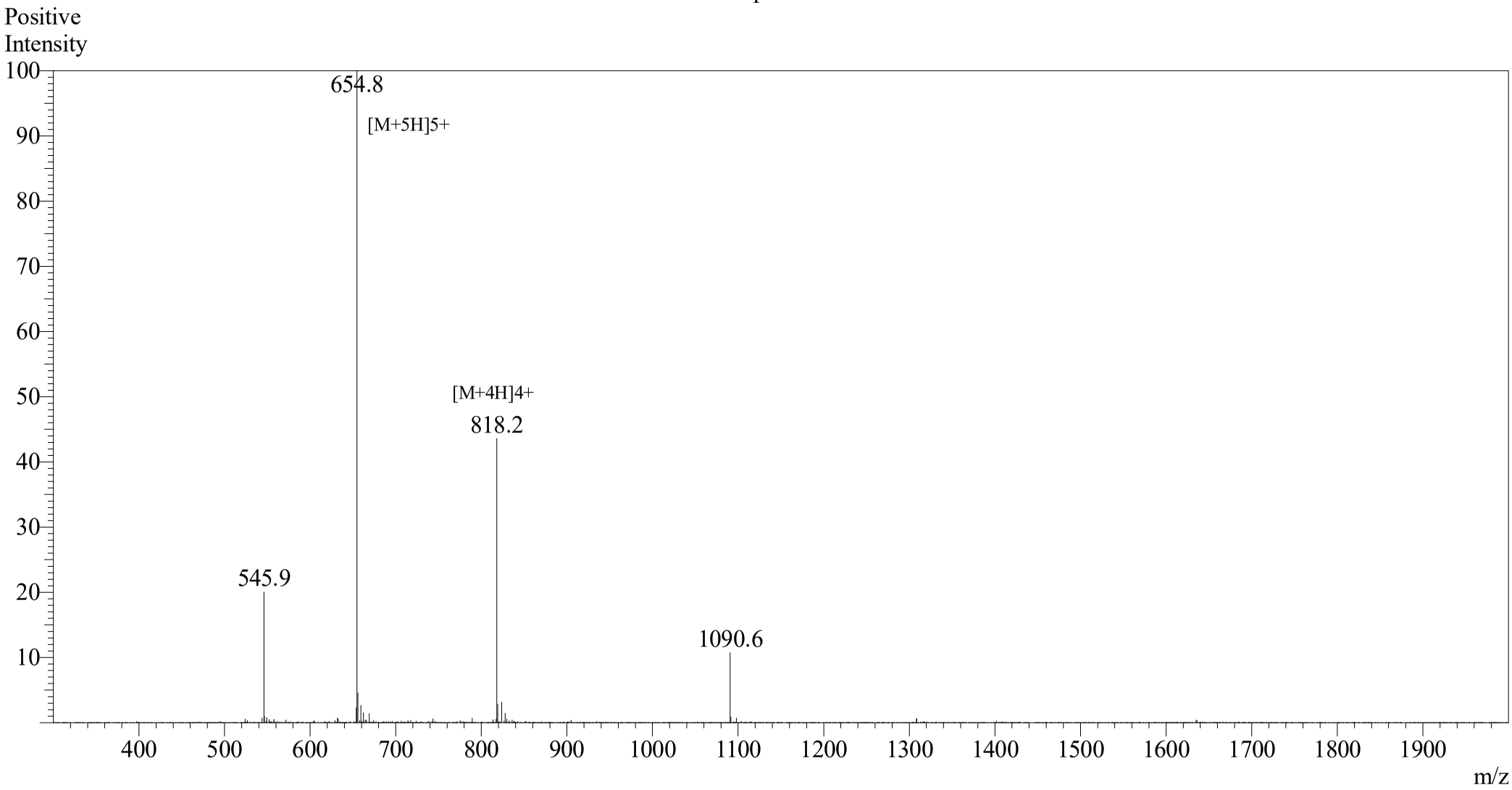

Sample Information

Acquired by :	Gary
Month-Day Processed :	03/17/20
Time Processed :	12:10:53 PM
Injection Volume :	0.3
Sample Name :	HS_Bim
Sample ID :	U6608FC030-3
Theoretical MW :	3269.67
Observed MW :	3269.0

Interface	:ESI
Nebulizing Gas Flow	:1.5L/min
CDL Temp	:250
Block Temp	:200

Equipment	: GK11010007
Interface Bias	: +4.5 kV
Drying Gas Flow	:5 L/min
T.Flow	:0.2 ml/min
B.conc	:50%H2O/50%MeOH

Mass Spectrum

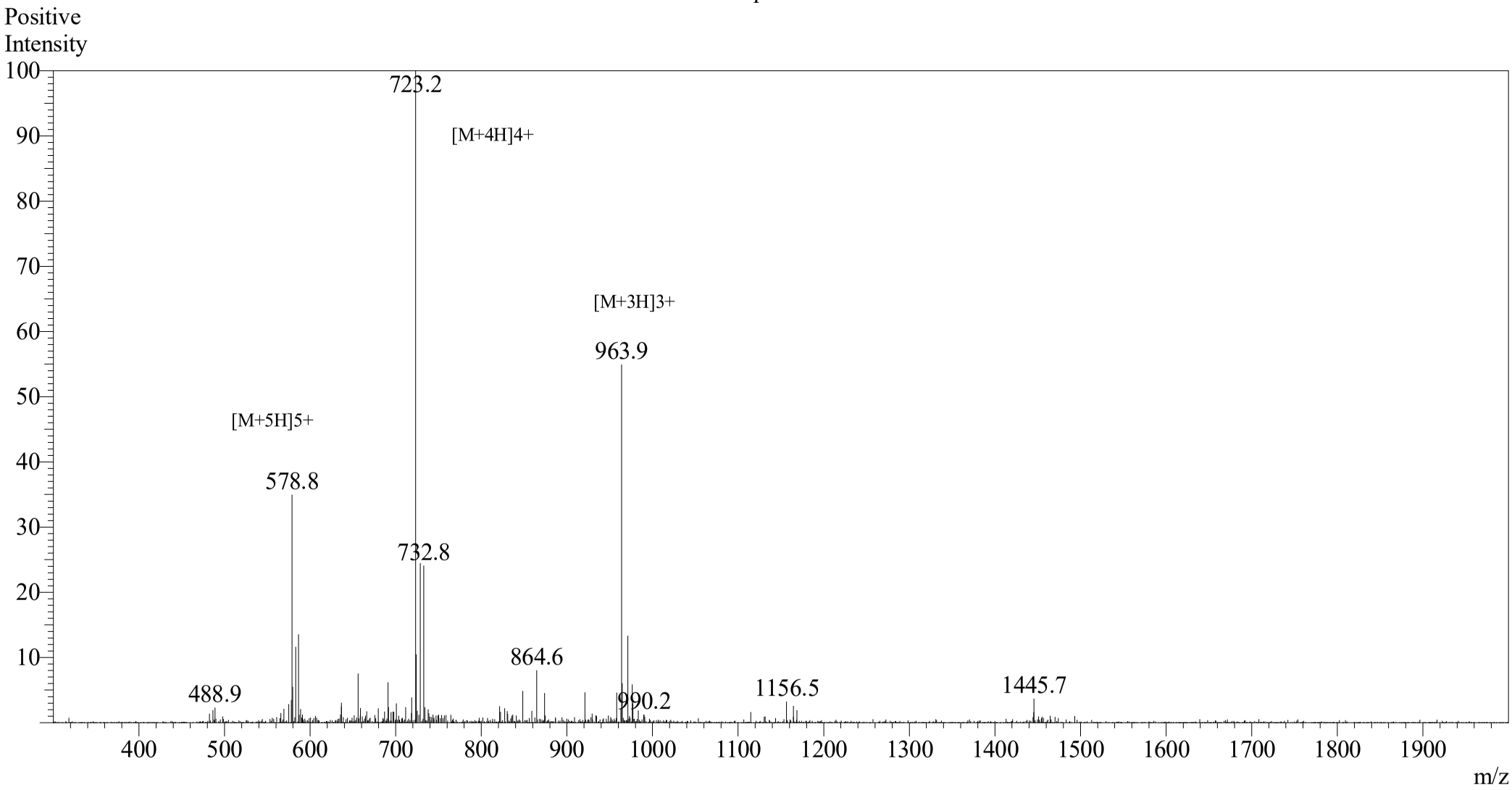

Sample Information

Acquired by :	Gary
Month-Day Processed :	03/22/20
Time Processed :	10:54:05 AM
Injection Volume :	0.3
Sample Name :	HS_Bid
Sample ID :	U6608FC030-5
Theoretical MW :	2889.22
Observed MW :	2888.8

Interface	:ESI
Nebulizing Gas Flow	:1.5L/min
CDL Temp	:250
Block Temp	:200

Equipment	: GK11010007
Interface Bias	: +4.5 kV
Drying Gas Flow	:5 L/min
T.Flow	:0.2 ml/min
B.conc	:50%H2O/50%MeOH

Mass Spectrum

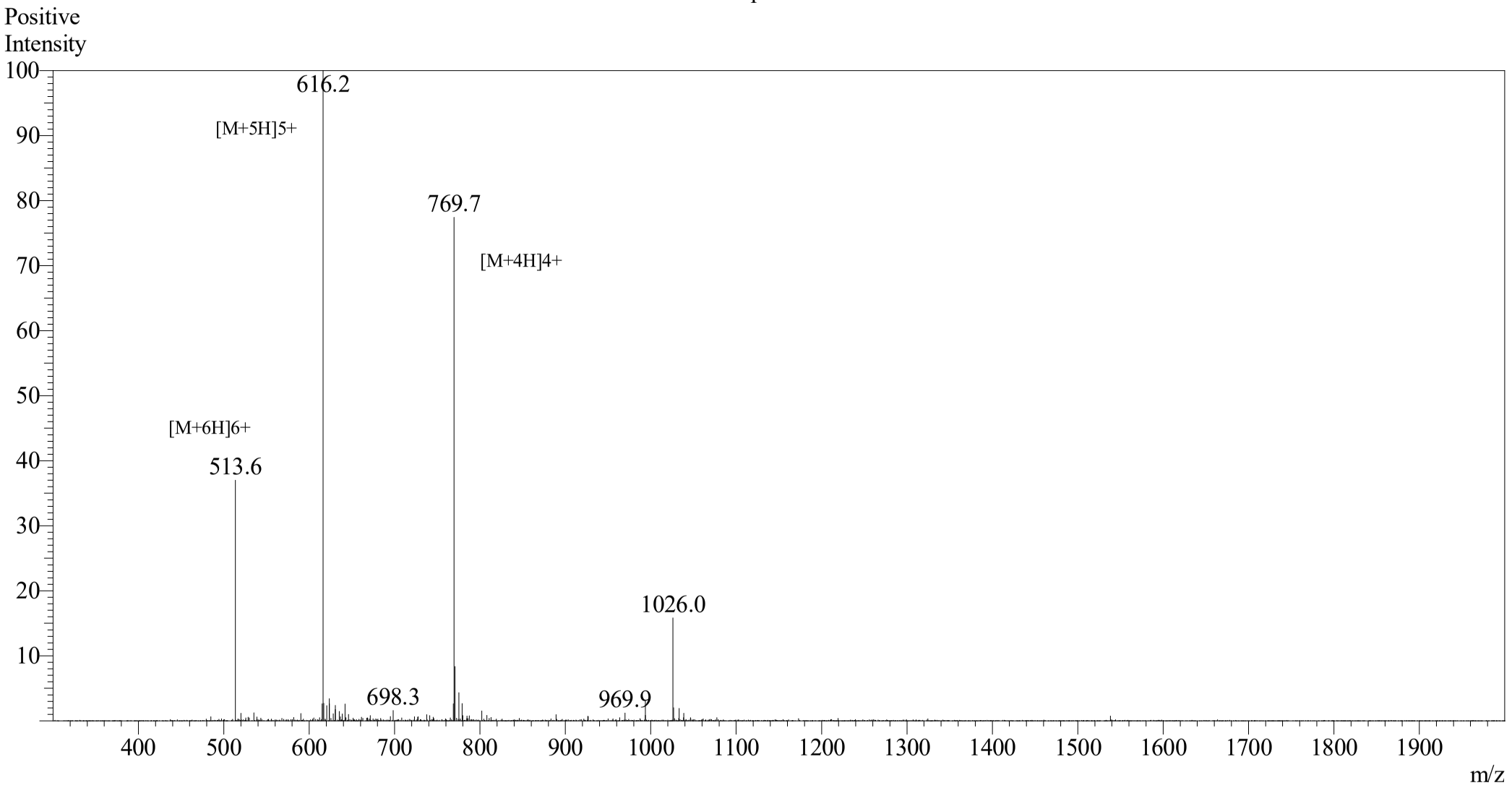

Sample Information

Acquired by :	Gary
Month-Day Processed :	03/17/20
Time Processed :	11:57:56 AM
Injection Volume :	0.3
Sample Name :	HS_Noxa
Sample ID :	U6608FC030-7
Theoretical MW :	3075.56
Observed MW :	3076.0

Interface	:ESI
Nebulizing Gas Flow	:1.5L/min
CDL Temp	:250
Block Temp	:200

Equipment	: GK11010007
Interface Bias	: +4.5 kV
Drying Gas Flow	:5 L/min
T.Flow	:0.2 ml/min
B.conc	:50%H2O/50%MeOH

Mass Spectrum

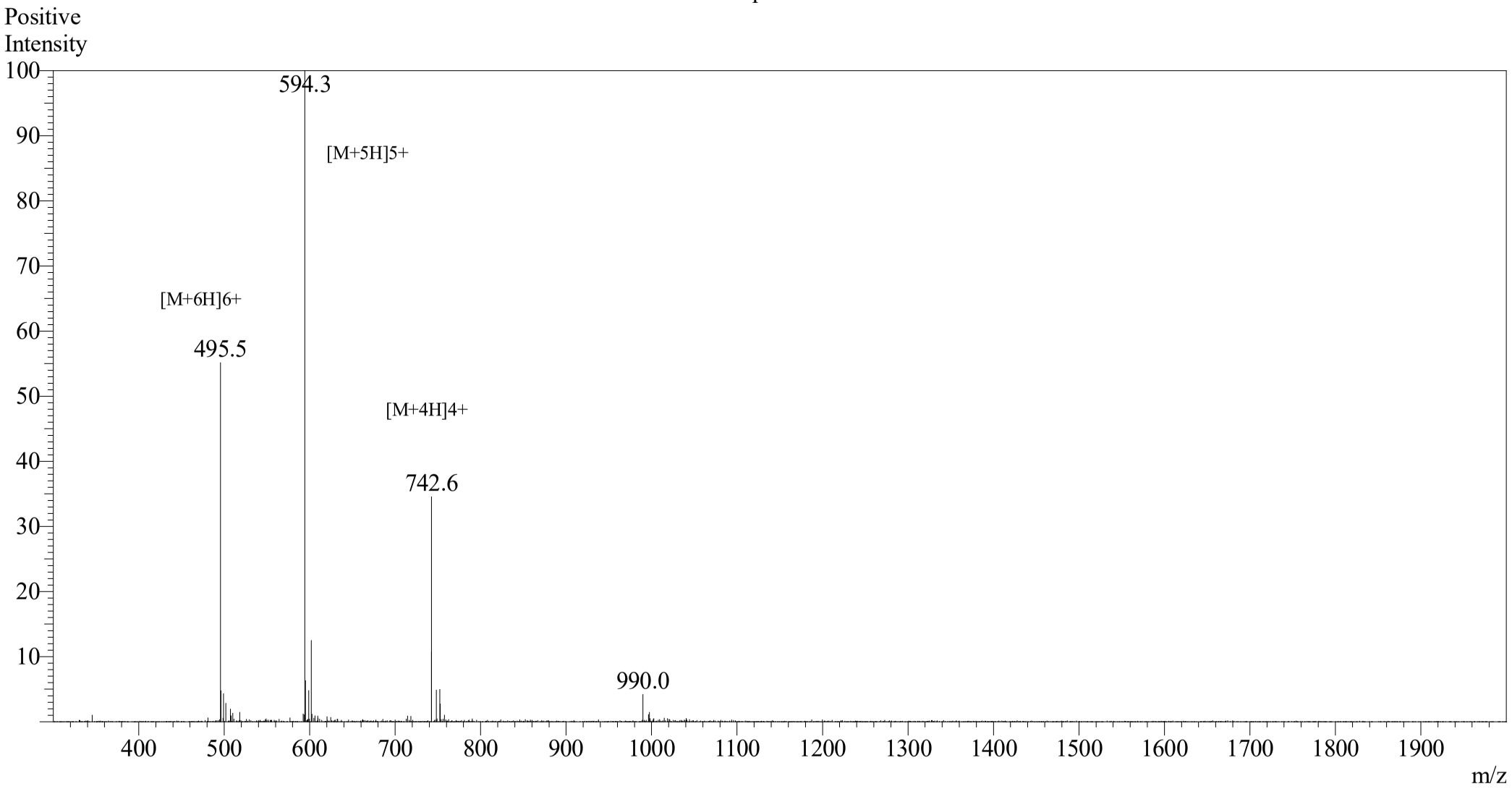

Sample Information

Acquired by :	Gary
Month-Day Processed :	03/26/20
Time Processed :	10:40:24 AM
Injection Volume :	0.3
Sample Name :	HS_Hrk
Sample ID :	U6608FC030-9
Theoretical MW :	2967.38
Observed MW :	2966.5

Interface	:ESI
Nebulizing Gas Flow	:1.5L/min
CDL Temp	:250
Block Temp	:200

Equipment	: GK11010007
Interface Bias	: +4.5 kV
Drying Gas Flow	:5 L/min
T.Flow	:0.2 ml/min
B.conc	:50%H2O/50%MeOH

Mass Spectrum

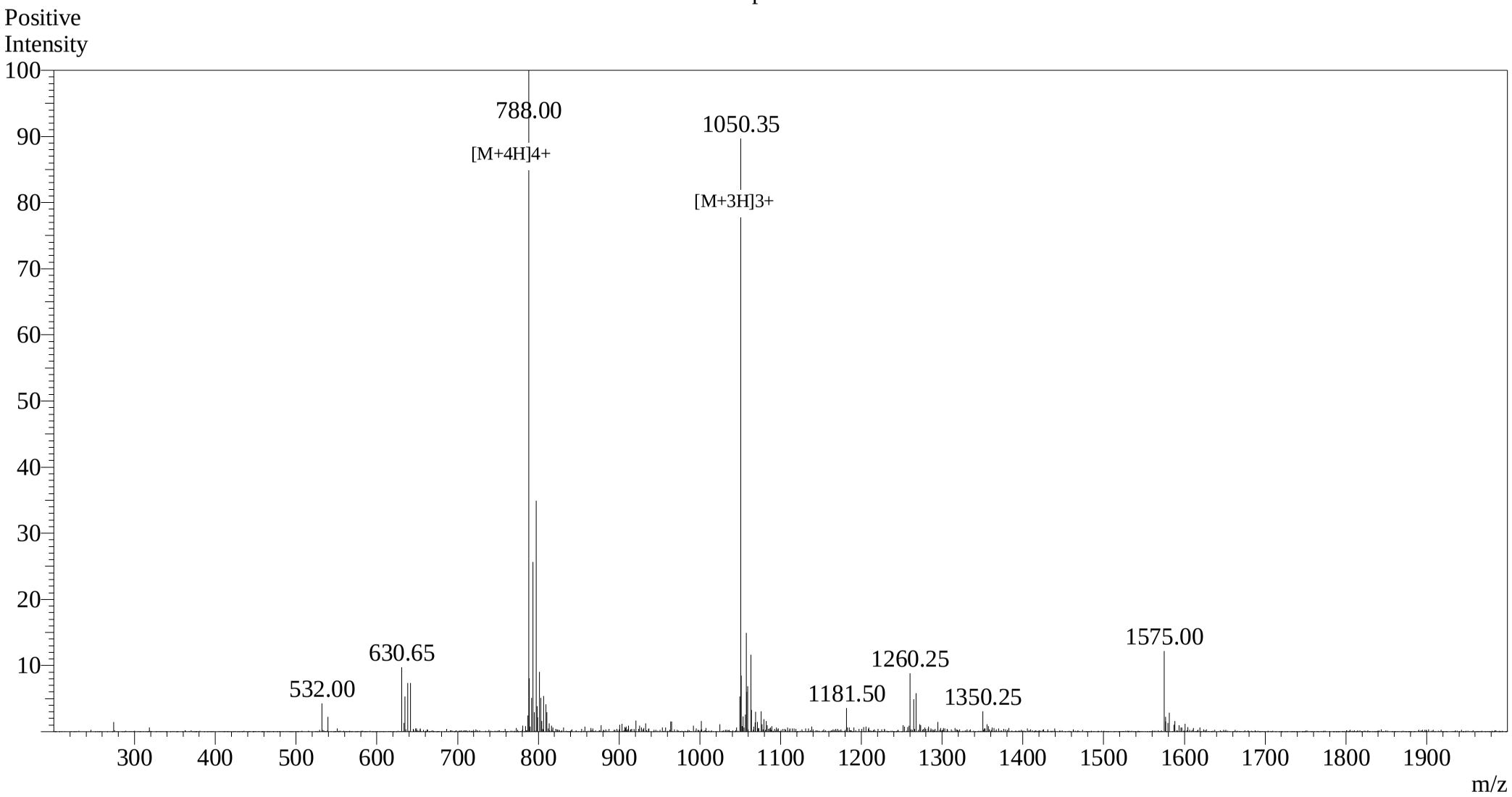

Sample Information

Acquired by :	Gary
Month-Day Processed :	12/21/14
Time Processed :	16:31:33
Injection Volume :	0.2
Sample Name :	hsBax
Sample ID :	520838-4
Theoretical MW :	3148.54
Observed MW :	3148.00

Interface	:ESI
Nebulizing Gas Flow	:1.5L/min
CDL Temp	:250℃
Block Temp	:200℃

Interface Bias	: +4.5 kV
Drying Gas Flow	:5 L/min
T.Flow	:0.2 ml/min
B.conc	:50%H2O/50%MeOH

Mass Spectrum

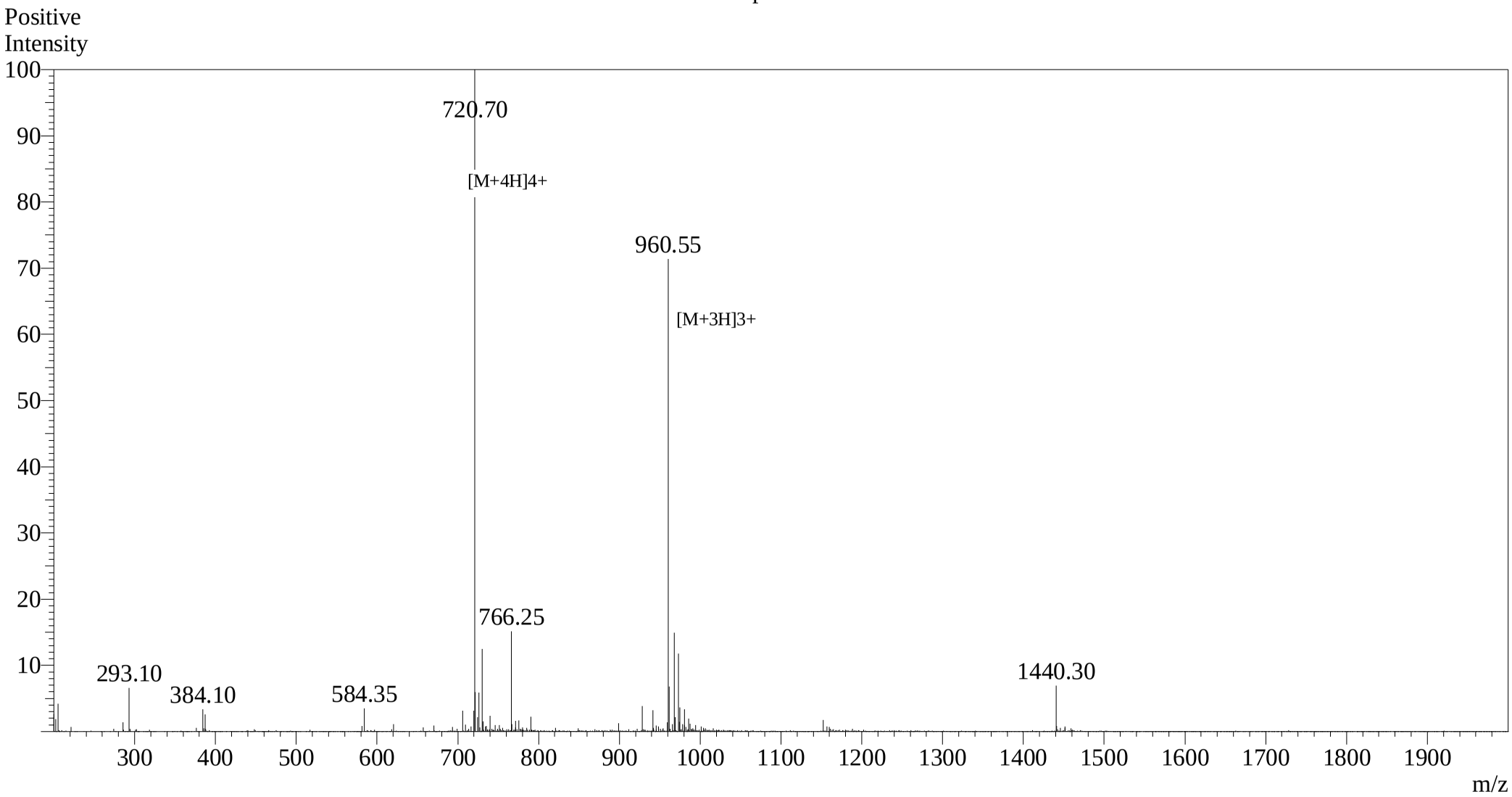

Sample Information

Acquired by :	Gary
Month-Day Processed :	12/03/14
Time Processed :	15:19:18
Injection Volume :	0.2
Sample Name :	hsBak
Sample ID :	520838-7
Theoretical MW :	2879.14
Observed MW :	2878.80

Interface	:ESI
Nebulizing Gas Flow	:1.5L/min
CDL Temp	:250℃
Block Temp	:200℃

Interface Bias	: +4.5 kV
Drying Gas Flow	:5 L/min
T.Flow	:0.2 ml/min
B.conc	:50%H2O/50%MeOH

Mass Spectrum

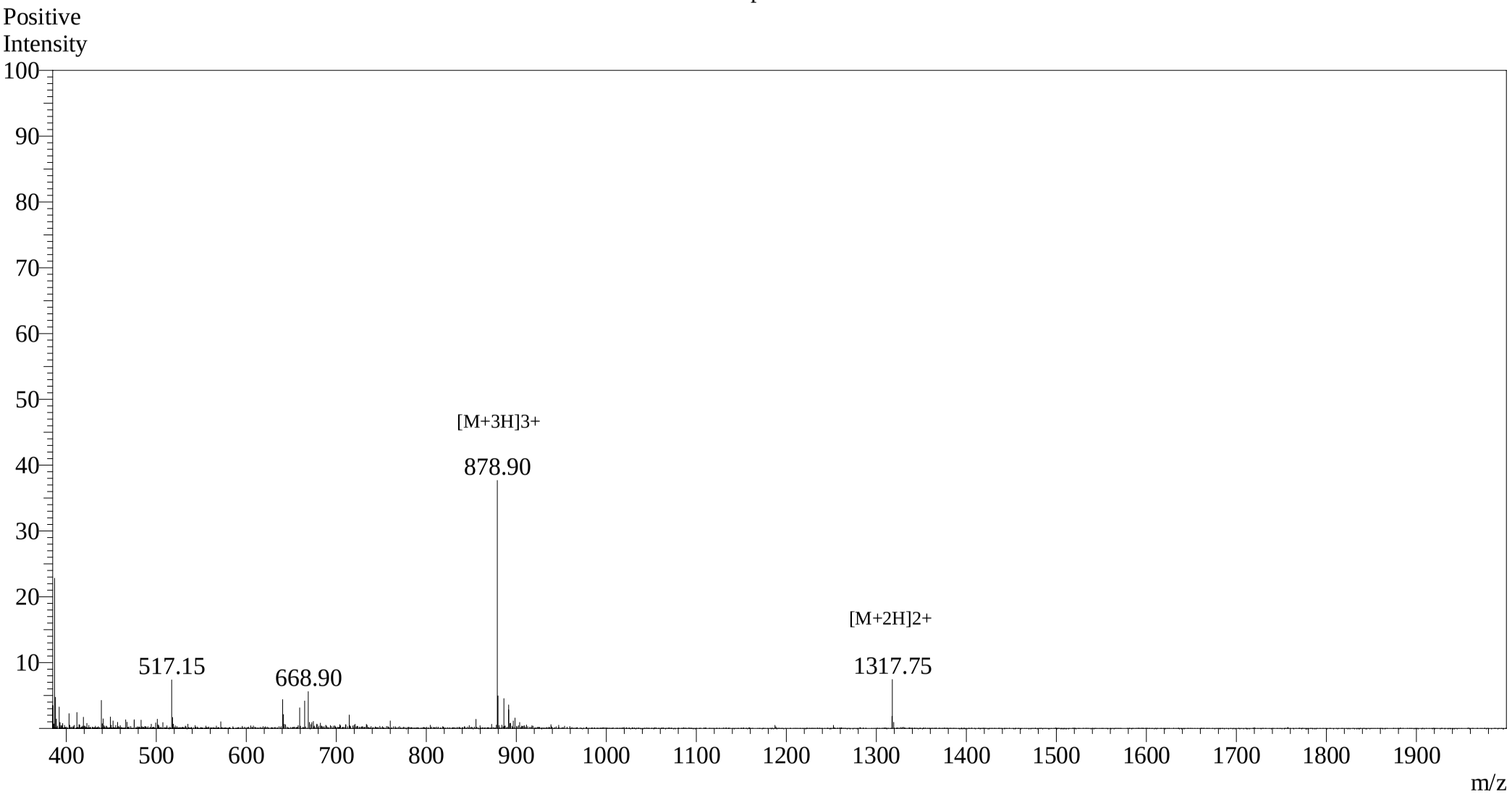

Sample Information

Acquired by :	Gary
Month-Day Processed :	01/15/15
Time Processed :	10:36:31
Injection Volume :	0.2
Sample Name :	hsBik
Sample ID :	529718-7
Theoretical MW :	2634.03
Observed MW :	2633.70

Interface	:ESI
Nebulizing Gas Flow	:1.5L/min
CDL Temp	:250℃
Block Temp	:200℃

Interface Bias	: +4.5 kV
Drying Gas Flow	:5 L/min
T.Flow	:0.2 ml/min
B.conc	:50%H2O/50%MeOH

Mass Spectrum

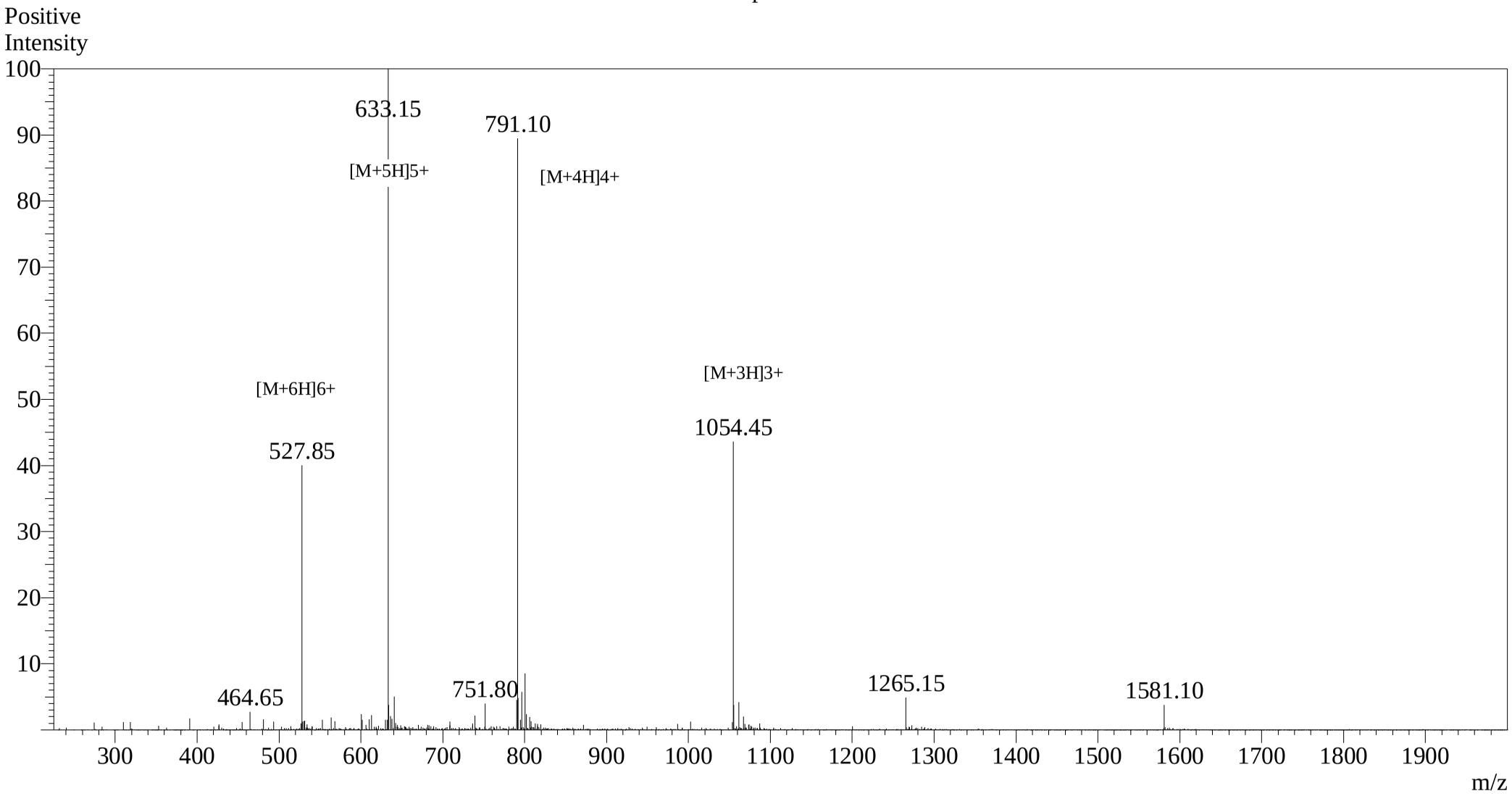

Sample Information

Acquired by :	Gary
Month-Day Processed :	04/12/15
Time Processed :	9:27:26
Injection Volume :	0.2
Sample Name :	hs_Bad
Sample ID :	584683-7
Theoretical MW :	3160.54
Observed MW :	3160.75

Interface	:ESI
Nebulizing Gas Flow	:1.5L/min
CDL Temp	:250℃
Block Temp	:200℃

Interface Bias	: +4.5 kV
Drying Gas Flow	:5 L/min
T.Flow	:0.2 ml/min
B.conc	:50%H2O/50%MeOH

Mass Spectrum

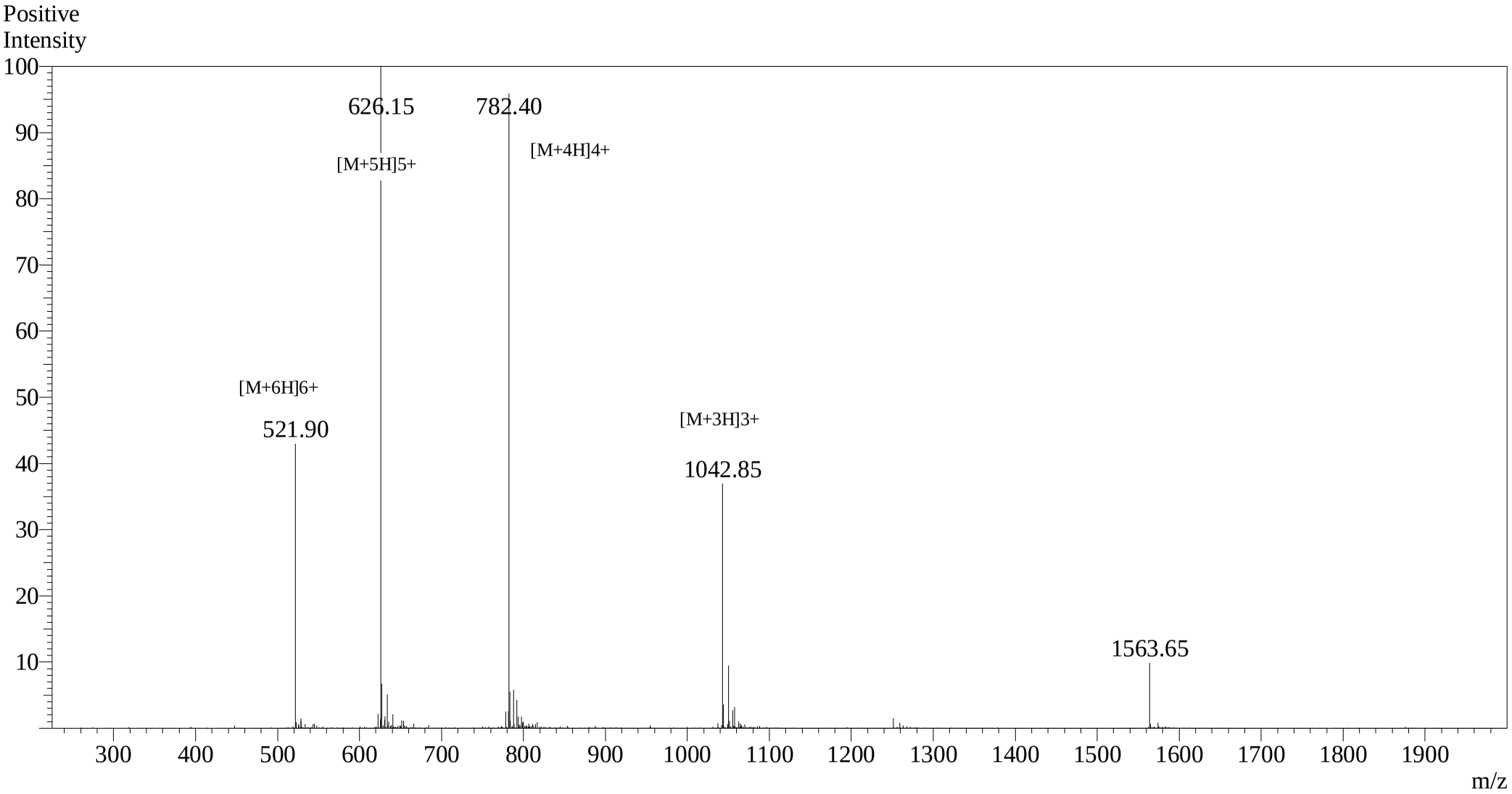

Sample Information

Acquired by :	Gary
Month-Day Processed :	04/10/15
Time Processed :	16:05:49
Injection Volume :	0.2
Sample Name :	hs_Bmf
Sample ID :	584692-3
Theoretical MW :	3125.54
Observed MW :	3125.75

Interface	:ESI
Nebulizing Gas Flow	:1.5L/min
CDL Temp	:250℃
Block Temp	:200℃

Interface Bias	: +4.5 kV
Drying Gas Flow	:5 L/min
T.Flow	:0.2 ml/min
B.conc	:50%H2O/50%MeOH

Mass Spectrum

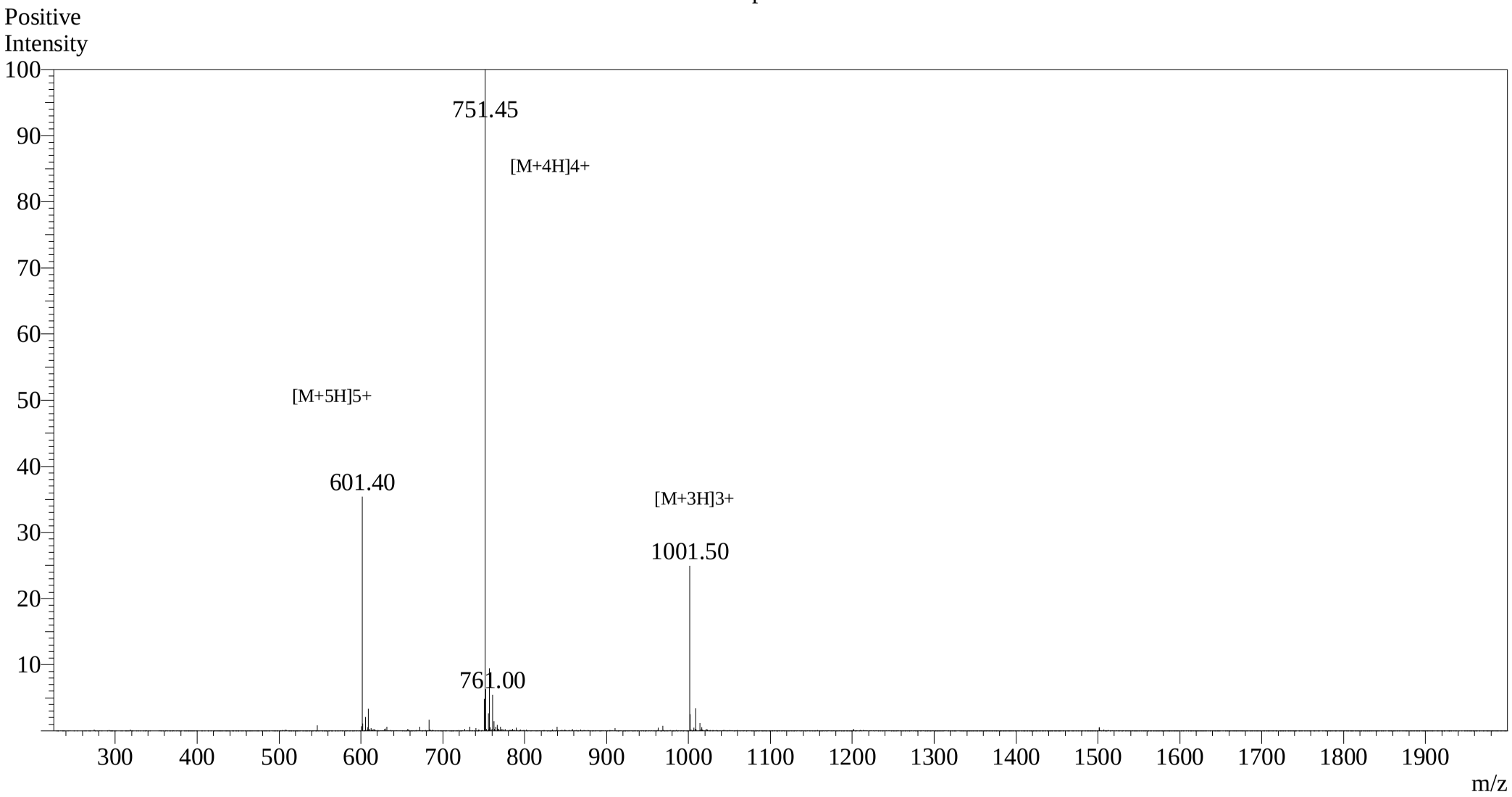

Sample Information	
Acquired by :	Gary
Month-Day Processed :	04/12/15
Time Processed :	17:22:15
Injection Volume :	0.2
Sample Name :	hs_Bok
Sample ID :	584692-5
Theoretical MW :	3001.54
Observed MW :	3001.80

Interface	:ESI
Nebulizing Gas Flow	:1.5L/min
CDL Temp	:250℃
Block Temp	:200℃

Interface Bias	: +4.5 kV
Drying Gas Flow	:5 L/min
T.Flow	:0.2 ml/min
B.conc	:50%H2O/50%MeOH